JULY, 2012

The ELI-D function as a tool to characterize the chemical bond in crystalline solids

Alfonso Gallo Bueno

Master Thesis

European Master in

Theoretical Chemistry and Computational Modelling

JULIO, 2012

La función ELI-D en el estudio del enlace químico en sólidos cristalinos

Alfonso Gallo Bueno

Tesis de máster

Máster europeo en

Química Teórica y Modelización Computacional

D. Ángel Martín Pendás, Catedrático del Departamento de Química Física y Analítica de la Universidad de Oviedo y Coordinador del Máster Europeo en Química Teórica y Modelización Computacional,

CERTIFICA:

Que el trabajo titulado **La función ELI en el estudio del enlace químico en sólidos cristalinos** ha sido realizado por Alfonso Gallo Bueno, bajo la tutela del catedrático D. Ángel Martín Pendás con el fin de optar al título que otorga el Máster Europeo en Química Teórica y Modelización Computacional.

Oviedo, 25 de julio de 2012

Fdo.: Ángel Martín Pendás
Coordinador del Máster Europeo en Química Teórica y Modelización Computacional

D. Ángel Martín Pendás, Catedrático de Química Física del Departamento de Química Física y Analítica de la Universidad de Oviedo,

CERTIFICA:

Que el trabajo titulado **La función ELI en el estudio del enlace químico en sólidos cristalinos**, ha sido realizado bajo su dirección por Alfonso Gallo Bueno, constituyendo su Tesis de Máster, cuya presentación autoriza.

Oviedo, 25 de julio de 2012

Fdo.: Ángel Martín Pendás

Aknowledgments

I wish to thank Ángel Martín Pendás for the inestimable teaching and help and for supervising my work dedicating me his time. Many thanks to Victor Luaña Cabal for the fruitful conversations. To Miroslav Kohout and Alexey Baranov for the prompt and inestimable help with the theoretical and computational dificulties. Thanks as well to Evelio Francisco Miguélez for carefully reading my work.

I want to express my gratitude to Nuno Galamba for receiving me in Lisbon, where I wish to return. Beautiful city, awesome people.

I also want to warmly thank my lab collegues Mamel, Miriam, David and Roberto for helping any time necessary and making a enjoyable atmosphere everyday. To pinche Marco and Alberto, to encourage them to return. Specially warm thanks to Marcos, my collegue of adventures during the master. I would like to send also a big hug to Ana, for being her.

Finally many thanks to David, for vehemently showing me his musical preferences in Valencia. A friend.

To my mother
To Tati y Tata, "¿qué tengo yo, que mi amistad procuras?"
L. de V.

Abstract

The Electron Localizability Indicator (ELI) is a scalar field able to resolve the atomic shell structure of atoms, molecules and solids. One of its specific forms ELI-D allows for partitioning of the space into extremely small space-filling non-overlapping regions enclosing a fixed amount of electron pair density. Such localization domains are of three types corresponding to the valence region —bonding regions—, the atomic core —non-bonding regions— or the lone pairs. Localization (LI) and Delocalization Indices (DI) result from the evaluation of the overlap integrals within such regions and yield information about how the valence electrons arrange forming covalent, ionic or metallic bonds. We have examined the performance of the ELI-D as computed with the DGrid code [1] in representative systems for metals (*bcc* K), ionic systems (NaF and LiCl) and semiconductors (SnTe) and compared it with the standard results of the Quantum Theory of Atoms In Molecules. As model systems of each type the crystals *bcc* K (metal), NaF and LiCl (ionic) and SnTe (covalent) were chosen. From the results obtained we can conclude that evaluation of LIs and DIs within ELI-D basins arises as a tool to quantitatively determine the nature of the chemical bond in crystal structures.

Contents

1. Introduction

Most of our chemical and physical knowledge of nature is sustained upon the invariant behaviour of interacting atoms or ions when forming part of different compounds. These atoms retain their individuality when they are transferred which confers the materials well-defined properties. When treating quantum-mechanically molecules or condensed phases a new and very different interpretation than the classical, traditional chemical undestanding has arisen, giving rise to the longly debated issue of how to recover the basic chemical concepts from quantum descriptions.

Atomic charges, chemical bonds, covalency, ionicity, resonance, etc., as examples among these traditional concepts, are firmly rooted for the chemist or physicist and exploited everyday in chemistry. Due to their relevance and importance much effort is being done to recover these concepts from multi-electron wave functions or to univocally define them. Moreover, it commonly happens that the quantities used to quantify these concepts tend to weaken or even disappear as the accuracy of wave functions increases.

Within this context, a new paradigm has arisen in the chemical interpretation of quantum mechanics since it became clear for the scientific community that sophisticated analyses based on the electron density, ρ, might give sound physical meaning to the aforementioned although fuzzy, yet chemically appealing concepts.

After Hohenberg and Kohn's theorem that was the first step towards the nowadays known as Density Functional Theory (DFT) [2], and the developement of the Quantum Theory of Atoms In Molecules (from now on referred to as QTAIM) by R.F.W. Bader [3], it was made possible to give rigorous physical interpretation to chemical bonding concepts through electron densities. The observable character of ρ, amenable to be experimentally determined, also helped to introduce this concept to a broad audience.

The need to partition physically every global system property into distinct, isolated contributions is so deeply rooted for the chemist and physicist. Traditional theories of bonding consist of partitioning the electron charge into the nuclear centers under study, usually by means of Mulliken analyses. Many of the interpretative models of chemical behaviour are based on very badly defined concepts, mainly dependent on a whole hierarchy of approximations.

Daudel and co-workers have reasoned that there should be some "best" decomposition of the physical space of a system into mutually exclusive regions called loges [4] and [5]. With "best" loges it was meant the most probable division of

the physical space of a system into localized groups of electons. The best loges were defined in a different sense by Bader *el al.* in [6]. In real space, the 3D partitioning of space induced by the topology of scalar fields like the electron density have provided a means to deal with the above-mentioned chemical notions. However, due to the sucess of the Electron Localization Function (ELF), it is becoming clearer that the electron density alone is not powerful enough to give solution to all of our most beloved chemical concepts. Most notions used in the work described here depend on quantum mechanical objects that cannot be derived from the electron density alone. Thus, density matrices from which not only one-particle but also two-particle properties such as the electron pair density D_2, may be derived need to be considered.

We will use in this work two procedures to partition space. The QTAIM method and the ω-restricted scheme of M. Kohout and coworkers. The former partition is coarse-grained and associates every spatial region usually with atoms; the latters fine-grained with extremely small and of variable size regions defined in such a way that a quantum mechanical property is conserved within them.

Based on the one-particle electron density $\rho(\boldsymbol{r})$, the partition of the space of the QTAIM imposes the condition that a region must be bounded by a surface whose flux of the gradient of the electron density $\vec{\nabla}\rho$ is zero. Regions subject to such constraint are called atomic *basins*, which are arranged fully occupying the whole volume under study and which are non-overlapping among each other. Each basin, in general, contains only one nucleus: it is usually assigned to an atom [3].

The use of the Fermi hole to measure the Fermi correlation has been pioneered by the works of Lennard-Jones [7] and Bader and Stephens[6]. On the other hand, I will also use a different partition of the space according to the quantity which named Electron Localizability Indicator (ELI), first introduced by M. Kohout [8]. ELI is a common name to a whole family of functionals describing the effect of local correlation of electronic motion in momentum [9] or coordinate space [8]. Here we will use one of its forms, ELI-D Υ_D^σ which is among the most common (for more detailed information about other ELI functionals see [8] and references therein). It is a so called ω-restricted space partitioning which consists on a space decomposition into a huge number of extremely small cells constrained through certain rules. A control function is chosen that determines the cell volumes by imposing the condition that they must enclose the same (infinitesimally) small fixed amount of the control quantity. Once the regions are defined a second sampling function is integrated within each region, whose discrete distribution is further examined [10]. In this work the ELI-D partition has been chosen, meaning that the electron pair density $\gamma(\boldsymbol{r}_1, \boldsymbol{r}_2)$ as a two-particle quantity is used as the control function whereas the electron density $\rho(\boldsymbol{r})$ is sampled over the regions.

Bader's own background has conditioned the diffusion of his theory, restricted mainly to molecular quantum chemistry, and seldom never applied to condensed matter (for some exceptions see the series [11], [12] and [13], and in [14]). Neither ELI-D has been yet much applied in solid state since it has been recently introduced and its implementation has just been achieved (an exception can be found in [15].

In this exploratory work we have chosen four different crystals to which QTAIM and ELI-D space partitioning has been applied: *bcc* K as a metal, NaF and LiCl as ionic crystals (insulators) and SnTe as semiconductor. Single point calculations at the experimental geometries of the above crystals have been done using the one-electron full-potential linearized augmented-plane wave (FP-LAPW) code Elk [16]. In the next step the output of Elk was processed by the DGrid program, developed by M. Kohout [1] to create a grid of the electron density and ELI-D values. From these grids the corresponding basins have been searched for and graphically represented. Over the resulting basins, according either to the electron density $\rho(\boldsymbol{r})$ or to the ELI-D indicator Υ_D^σ, fluctuations, localization and delocalization indices have been evaluated from overlap integrals and used to characterize the bonding situation of the crystals.

The structure of the present work is as follows: in Chapter 1 the theoretical methodology used at every step to finally calculate the indices is briefly presented, from the Schrödinger equation to the bond descriptors of the chemical bond in real space QTAIM and ELI-D. In Chapter 2, the computational methods and resources used in the different calculations are described. Chapter 3 presents the results for the 4 systems: the critical points (for 3 of the 4 systems), a pictorical representation of the basins and the localization and delocalization indices as well as electron population fluctuations. Finally in Chapter 4 a number of conclusions are gathered.

2. Theoretical methods

2.1. Many electrons wave functions and the Schrödinger equation

In quantum mechanics, all the information we can possibly have about a system is contained in the system's wave function Ψ. The calculation of the wave function not considering relativistic effects nor time dependency consists on solving the Schödinger equation:

$$\hat{H}\Psi = E\Psi. \tag{2.1}$$

E is the energy of the system, which results from applying the Hamiltonian operator $\hat{H}$ to the aforementioned wave function Ψ. When considering a many-body problem, i.e., having more than one electron, equation 2.1 becomes:

$$\hat{H}\Psi(\boldsymbol{r}_1, \boldsymbol{r}_2 \ldots, \boldsymbol{r}_N) = E\Psi(\boldsymbol{r}_1, \boldsymbol{r}_2 \ldots, \boldsymbol{r}_N), \tag{2.2}$$

where electron 1 is located at position $\boldsymbol{r}_1$, electron 2 at $\boldsymbol{r}_2$ and so on. The Hamiltonian operator $\hat{H}$ for a system consisting on M nuclei and N electrons described by position vector R_A and r_i, respectively, addopts the form:

$$\hat{H} = -\sum_{i=1}^{N}\frac{1}{2}\nabla_i^2 - \sum_{A=1}^{M}\frac{1}{2M_A}\nabla_A^2 - \sum_{i=1}^{N}\sum_{A=1}^{M}\frac{Z_A}{r_{iA}} + \sum_{i=1}^{N}\sum_{j>i}^{N}\frac{1}{r_{ij}} + \sum_{A=1}^{M}\sum_{B>A}^{M}\frac{Z_A Z_B}{R_{AB}}. \tag{2.3}$$

The M nuclei and N electrons are designated by A, B and i, j, respectively. Nucleus A has the nuclear charge Z_A while M_A is the ratio of its mass to the mass of an electron, all in atomic units. The Laplacian operators ∇_i^2 and ∇_A^2 involve second derivation with respect of the space coordinates of the ith electron and the Ath nucleus.

The first two terms in the previous equation describe the kinetic energy of electrons and nuclei, respectively. The remaining three terms are the potential of the Hamiltonian and represent the attractive electrostatic interaction nucleus-electron and the potential describing the repulsion nucleus-nucleus and electron-electron, respectively.

In our case we will be concerned only with the electronic structure of matter,

more precisely of solids. Hence the expression for the system's Hamiltonian Eq. 2.3 can be further simplified by means of the well known Born-Oppenheimer approximation. The mass of an electron is very small compared to that of a nucleus [1]. That big difference between both particle masses makes the electrons move much faster than nuclei do, which allows us to approximate the speed of the nuclei as if they were static. Within the Born-Oppenheimer approximation electrons are considered to move within a field of fixed nuclei and therefore the nuclear kinetic energy (second term in Eq. 2.3) vanishes. The last term, which accounts for the nucleus-nucleus repulsion can be considered to be constant. Since, according to the quantum mechanics rules, the addition of a constant to an operator only adds to the operator eigenvalues but leaves the eigenfunctions unaffected, this term can also be neglected:

$$\hat{H}_{elec} = -\sum_{i=1}^{N} \frac{1}{2}\nabla_i^2 - \sum_{i=1}^{N}\sum_{A=1}^{M} \frac{Z_A}{r_{iA}} + \sum_{i=1}^{N}\sum_{j>i}^{N} \frac{1}{r_{ij}} = \hat{T} + \hat{V}_{Ne} + \hat{V}_{ee}, \tag{2.4}$$

which is the electronic Hamiltonian describing the motion of N electrons in the field of M nuclei now represented by point charges. The Schödinger equation becomes now:

$$\hat{H}_{elec}\Psi_{elec} = E_{elec}\Psi_{elec}, \tag{2.5}$$

where the electronic energy E_{elec} results from the application of the electronic Hamiltonian $\hat{H}_{elec}$ on the electronic wave function Ψ_{elec}. And of course the total energy is found as:

$$E_{tot} = E_{elec} + E_{nuc}. \tag{2.6}$$

A more detailed description of the nuclear part of the Schrödinger equation and the total Hamiltonian can be found anywhere in the literature, as for example [17, 18].

2.1.1. The antisymmetry or Pauli exclusion principle

To completely describe an electron we would need to consider not only its spatial but also its spin coordinates. The wave function will then be $\Psi(\boldsymbol{x}_1, \boldsymbol{x}_2 \ldots, \boldsymbol{x}_N)$, where $\boldsymbol{x}_1 = (\boldsymbol{r}_1, \sigma_1)$ are the spatial and spin coordinates, respectively.

The wave function itself is not observable. The only physical interpretation that can be obtained out of it is related to the square of it, that yields the probability of finding electron 1 in $d\boldsymbol{x}_1$, 2 in $d\boldsymbol{x}_2$, ... and N in $d\boldsymbol{x}_N$, simultaneously:

[1] The nucleus-electron mass ratio for the lightest nucleus (proton ^{1}H) is of 1,800. For very common atoms as C, the ratio is increased to 20,000.

$$|\Psi(\boldsymbol{x}_1, \boldsymbol{x}_2 \ldots \boldsymbol{x}_N)|^2 d\boldsymbol{x}_1 d\boldsymbol{x}_2 \ldots d\boldsymbol{x}_N. \tag{2.7}$$

For indistiguishable particles this probability does not change if the coordinates of two of them are exchanged. The nature offers two possibilities regarding the permutation of the coordinates of two particles: either the resulting wave function is identical, in which case we are considering *bosons* or it is antysimmetric (has opposite sign), and then we are facing *fermions*. Electrons are fermions with spin = 1/2 and the wave function Ψ is antysimmetric:

$$\Psi(\boldsymbol{x}_1, \boldsymbol{x}_2 \ldots \boldsymbol{x}_N) = -\Psi(\boldsymbol{x}_2, \boldsymbol{x}_1 \ldots \boldsymbol{x}_N). \tag{2.8}$$

The last expression is the quantum-mechanical generalization of the Pauli exclusion principle. The system wave function will be of course normalized, being the probability to find the N electrons in the whole space equal to the unity:

$$\int |\Psi(\boldsymbol{x}_1, \boldsymbol{x}_2 \ldots \boldsymbol{x}_N)|^2 d\boldsymbol{x}_1 d\boldsymbol{x}_2 \ldots d\boldsymbol{x}_N = 1. \tag{2.9}$$

2.1.2. The Hartree-Fock approximation

In the search for approximate solutions to the electronic Schrödinger equation as described in Eq. 2.5 the Hartree-Fock procedure still represents not only the corner stone of all conventional, i.e., wave function based quantum chemical methods, but also a conceptually very relevant theory as a first step towards more accurate approximations.

The simplest antisymmetric, i.e., fulfilling the Pauli exclusion principle wave function describing the ground state (indicated by the subindex) of an N-electron system, is a single Slater determinant[2]:

$$|\Psi_0\rangle = |\chi_1 \chi_2 \cdots \chi_N\rangle, \tag{2.10}$$

where χ_i are spin orbitals [3]. The variational principle states that the best wave function satisfying the above equation that can be found is the one which yields

[2] For a system with just two electrons occupying spin orbitals χ_i and χ_j a normalized linear combination of both spin orbitals can be found, in such a way that the antisymmetry principle is satisfied:

$$\Psi(\boldsymbol{x}_1, \boldsymbol{x}_2) = 2^{-1/2}\big(\chi_i(\boldsymbol{x}_1)\chi_j(\boldsymbol{x}_2) - \chi_j(\boldsymbol{x}_1)\chi_i(\boldsymbol{x}_2)\big).$$

This linear combination can be written as a determinant into what is known as a Slater determinant. It can easily be generalized for a N-electron system.

$$\Psi(\boldsymbol{x}_1, \boldsymbol{x}_2) = 2^{-1/2} \begin{vmatrix} \chi_i(\boldsymbol{x}_1) & \chi_j(\boldsymbol{x}_2) \\ \chi_i(\boldsymbol{x}_2) & \chi_j(\boldsymbol{x}_1) \end{vmatrix}.$$

[3] Spin orbitals *are one-electron functions built from a spatial orbital* $\phi_i(\boldsymbol{r})$ *and one of the two*

the lowest energy:

$$E_0 = \langle \Psi_0 | H | \Psi_0 \rangle. \tag{2.11}$$

The variational flexibility that will allow us to find the wave function with the lowest associated energy resides within the choice of spin orbitals. The energy E_0 has to be variationally minimized with respect to the choice of spin orbitals. An eigenvalue equation is derived, termed the Hartree-Fock equation, which determines the optimal eigenvalues:

$$f(i)\chi(\boldsymbol{x}_i) = \varepsilon(i)\chi(\boldsymbol{x}_i). \tag{2.12}$$

$f(i)$ is an effective one-electron operator known as *Fock* operator and $\varepsilon(i)$ is the corresponding energy for this state. The Hartree-Fock approximation consists of a substitution of the complicated many-body problem into a more simple one-electron situation, in which the electron-electron repulsion is averaged. The electronic Hamiltonian in Eq. 2.4 is transformed approximating the last term, which accounts for the electron-electron repulsion by a potential:

$$f(i) = -\frac{1}{2}\nabla_i^2 - \sum_{A=1}^{M} \frac{Z_A}{r_{iA}} + v_i^{HF}, \tag{2.13}$$

where the sum over the N electrons has been removed since the Fock operator $f(i)$ is already defined for ith electron. v_i^{HF} is the average potential experienced by the electron i due to the influence of the remaining electrons.

Explicitly, v_i^{HF} is composed by the two components:

$$v^{HF}(\boldsymbol{x}_1) = \sum_{j}^{N} \Big(\hat{J}_j(\boldsymbol{x}_1) - \hat{K}_j(\boldsymbol{x}_1) \Big). \tag{2.14}$$

The first term has the form:

$$v_i^{coul}(\boldsymbol{x}_1) = \sum_{j \neq i} \int \left|\chi_j(\boldsymbol{x}_2)\right|^2 \frac{1}{r_{12}} d\boldsymbol{x}_2. \tag{2.15}$$

It has a clear meaning. Electron i is described by the spin orbital χ_i and experiences a one-electron coulomb potential. This potential is dependent on the instantaneous position of electron 2 within χ_j, the region it occupies. It is hence a two-electron potential. However if we average the interaction r_{12}^{-1} between electron

spin functions $\alpha(s)$ or $\beta(s)$:

$$\chi(\boldsymbol{x}) = \phi_i(\boldsymbol{r})\sigma(s)$$
$$\sigma = \alpha, \beta$$

1 and electron 2 integrating over all space and spin coordinates $\boldsymbol{x}_2$ of electron 2, the two-electron potential is transformed into a one-electron potential by doing an average. The interaction between electrons 1 and 2 are weighted by the probability $d\boldsymbol{x}_2\big|\chi_j(\boldsymbol{x}_2)\big|^2$ of electron 2 to be found in the volume element $d\boldsymbol{x}_2$. Nevertheless the electron located at χ_i suffers all interactions arising from the $N-1$ electrons. By summing over $j \neq i$ spin orbitals, the total averaged potential acting on the electron in χ_i is obtained. A coulomb operator can be defined neglecting the sum, which adopts the form:

$$\hat{J}_i(\boldsymbol{x}_1) = \int \big|\chi_j(\boldsymbol{x}_2)\big|^2 \frac{1}{r_{12}} d\boldsymbol{x}_2, \tag{2.16}$$

which is the average local potential at $\boldsymbol{x}_1$ due to the electron located at χ_j.

The second term in Eq. 2.14 is called the exchange contribution to the HF potential. It arises from the antisymmetry of the single determinant and has no classical meaning. It can only be understood through its effect when operating on a spin orbital:

$$\hat{K}_j(\boldsymbol{x}_1)\chi_i(\boldsymbol{x}_1) = \Big[\int \chi_j^*(\boldsymbol{x}_2) r_{12}^{-1} \chi_i(\boldsymbol{x}_2) d(\boldsymbol{x}_2)\Big]\chi_j(\boldsymbol{x}_1). \tag{2.17}$$

It can be seen comparing the previous equation with Eq. 2.16 that the action of $\hat{K}$ produces an exchange of the variables in the two spin orbitals. Now χ_i is related to $\boldsymbol{x}_2$, and the result of the application of the exchange operator depends on the value of χ_i in all points of space. It is hence said to be *nonlocal* unlike the coulomb operator.

The potential v_i^{HF} seen by electron i depends on the spin orbitals of the remaining electrons. In other words, the Fock operator depends on its own eigenfunctions. Thus we need to know the solution to solve the equation. The problem has to be solved by means of an iterative procedure named Self-Consistent-Field method.

Every SCF loop starts with a initial guess of the spin orbitals that allows for the calculation of the mean potential v_i^{HF} seen by each electron. Eq. 2.12 is then solved and a new set of spin orbitals obtained, from which a new field v_i^{HF} is found closing one SCF loop and starting the iteration again until convergence in the χ's and ε's is attained (a schematic description of the SCF iterative process can be seen in Fig. 2.1).

We have already mentioned that the second term in Eq. 2.4 is also a potential that describes the interaction electron-nucleus. The spatial arrangement of the nuclei is the unique part of the whole equation that changes with the system under consideration. Hence whether our system is a solid, a molecule or an atom

is determined by the spatial arrangement of the nuclei, which is specified in the potential $v(\boldsymbol{x})$ accounting for the electron-nucleus interaction.

Electron correlation

The Hartree-Fock approximation simplifies the problem by treating the many-body problem as an effective single-body one. Thus, the HF approach neglects most of the correlation that exists between electrons. Electron correlation arises from the instantaneous repulsion of electrons which is not treated by the effective HF potential. Since the electron-electron interaction is considered as an average the electrons approach too much to each other leading to a higher repulsion than in the real situation. Consequently the HF system is less stable than it really is $|E_{HF}| < |E_0|$. The correlation energy will be the energy difference between the exact, non-relativistic energy and the HF system

$$E_{corr} = E_0 - E_{HF}. \tag{2.18}$$

Correlated energies have usually two different contributions. The first one, related to the motion of electrons, is called *dynamic correlation*. In many instances, however, a one Slater determinant description is not possible even in the simplest approximation, i.e., when degenerate or quasi-degenerate states exist. This is called *static correlation*.

In spite of its inherent errors the HF theory is still widely used due to its not too demanding computational requirements. For further and more detailed description of the fundamentals of Quantum Mechanics as well as HF and methods beyond HF, the reader is referred to the writings used to compose this Chapter [19], [20], [17] and [21].

2.2. Pos-Hartree-Fock methods: Density Functional Theory

The wave function of a system depends on 4N variables (3 spatial and 1 spin coordinates) which makes it a complicated object only able to be fully analyzed in very small systems, and hence automatically excluding most of the systems of interest in biology, material sciences, etc. In addition, this complexity increases the difficulty of having a clear description of the system and makes it hard to find an intuitive interpretation. On the other hand, the Hamiltonian of the system $\hat{H}$ is at most dependent on 2-particle operators, which suggests that the high complexity of the wave function contains redundant information that does not need to be considered

$$\hat{H}_{elec} = \underbrace{\hat{T} \quad + \quad \hat{V}_{Ne}}_{1-particle} \quad + \quad \underbrace{\hat{V}_{ee}}_{2-particle} \quad .$$

Using the electron density ρ —a real space quantity depending on only 3 coordinates— as an alternative option to solve the Schrödinger equation makes it possible, in principle, to overcome these problems.

2.2.1. First Hohenberg-Kohn theorem

Many attempts were performed in order to find a practical way of solving the Schrödinger equation using ρ. The most successful one is established by the first Hohenberg-Kohn theorem.

The electron density ρ is firstly proved to be a suitable quantity to solve the Schrödinger equation (Eq. 2.1) in the paper published by Hohenberg and Kohn in 1964 [2]. It —quoting literally [2]— states that "*the external potential* $V_{ext}(\boldsymbol{r})$*) is (to within a constant) a unique functional of* $\rho(\boldsymbol{r})$*; since in turn* $V_{ext}(\boldsymbol{r})$ *fixes* $\hat{H}$ *we see that the full many body particle ground state is a unique functional of* $\rho(\boldsymbol{r})$". A proof for this statement is easily done by *reductio ad absurdum*. A sketch runs as follows:

$$\rho_0 \longrightarrow \left\{\mathrm{N}, \mathrm{Z_A}, \mathrm{R_A}\right\} \longrightarrow \hat{H} \longrightarrow \Psi_0 \longrightarrow \mathrm{E}_0 \tag{2.19}$$

The electron density ρ_0 uniquely determines the hamiltonian of the system $\hat{H}$, and consequently both the wave function Ψ_0 and the energy E_0 of the system in its ground state are fully determined by the electron density, as well as all the properties of the system. But since $\hat{H}$ is the same for any state, all states of the system are as well determined by the ground state electron density ρ_0.

$$\mathrm{E}_0[\rho_0] = \int \underbrace{\rho_0(\boldsymbol{r})\mathrm{V}_{Ne}d\boldsymbol{r}}_{\text{System dependent}} + \underbrace{\mathrm{T}[\rho_0] + \mathrm{E}_{ee}[\rho_0]}_{\text{Universal}}. \tag{2.20}$$

From the above equation it can be seen that as the electron kinetic energy T as the electron-electron repulsion V_{ee} are independent of the considered system. However the term accounting for the electrostatic interaction nucleus-electron V_{Ne} is what determines which kind of system is being treated. Eq. 2.20 can be rewritten, including the universal part into a new functional: the *Hohenberg-Kohn functional*:

$$E_0[\rho_0] = \int \rho_0(\boldsymbol{r}) V_{Ne} d\boldsymbol{r} + F_{HK}[\rho_0]. \tag{2.21}$$

F_{HK} is the part which remains unchanged no matter the system. Apart from the electron kinetic energy T it contains information about the electron-electron interaction:

$$E_{ee}[\rho] = \frac{1}{2} \int d\boldsymbol{r}_1 \int \frac{\rho(\boldsymbol{r}_1)\rho(\boldsymbol{r}_2)}{r_{12}} d\boldsymbol{r}_2 + E_{ncl}[\rho]. \tag{2.22}$$

The first term is the classical part of the equation, called the Coulomb repulsion $J[\rho]$. The second part $E_{ncl}[\rho]$ is *non-classical* and accounts for the self-interaction correction and the interparticle correlation.

2.2.2. Second Hohenberg-Kohn theorem

We already know by the first H-K theorem that the ground state electron density suffices to determine any of the properties of the system. The next step, also solved by Hohenberg and Kohn in [2], is to ensure that the electron density ρ we are using is indeed the density of the ground state that we are looking for. In that sense the second H-K theorem establishes that the energy E_0 delivered by the H-K functional will be the lowest only if the density ρ is the density of the ground state ρ_0. This theorem is a variational principle which can be expressed as

$$E_0 = \min_{\Psi \to N} \langle \Psi | \hat{T} + \hat{V}_{Ne} + \hat{V}_{ee} | \Psi \rangle. \tag{2.23}$$

In other words, for any trial density the E obtained is an upper limit to the true ground state energy E_0:

$$E_0 \leq E[\rho] = T[\rho] + E_{Ne}[\rho] + E_{ee}[\rho]. \tag{2.24}$$

2.2.3. The Kohn-Sham Approach

Many attempts have been performed to attain a practical solution to the H-K equation 2.21. The most successful one is formulated in the second most important article within the developement of the density functional theory by W. Kohn

and L. Sham in 1965 [22].

The success of this new approach starts by considering that most of the problems making DFT inaccurate were related to the way the kinetic energy is treated. In their article, Kohn and Sham proposed a Hartree-Fock-like method —since the kinetic energy is more exactly determined within this approach— to more accurately calculate the kinetic energy. A part of it is then determined exactly by introducing the concept of a non-interacting reference system built from a set of orbitals (one-electron functionals), i.e., the electrons are treated as non-interacting fermions. The remaining contribution to the kinetic energy, a small part of the total, is treated by a non-classical approximate functional.

Kohn-Sham orbitals

The HK functional, expressed in equation 2.21 has the form

$$\mathrm{F}[\rho(\boldsymbol{r})] = \mathrm{T}[\rho(\boldsymbol{r})] + \mathrm{J}[\rho(\boldsymbol{r})] + \mathrm{E}_{ncl}[\rho(\boldsymbol{r})]. \tag{2.25}$$

$\mathrm{J}[\rho]$ is a classical term and can be exactly determined but the other two terms remain unkown. Regarding the kinetic energy $\mathrm{T}[\rho]$ it became clear that it was not properly described by the simple expression used by other approaches such as the Thomas-Fermi-Dirac model (see [18] for further information on alternative methods to the Kohn-Sham one).

The Kinetic energy is now treated by a hamiltonian of a non-interacting system in which the electrons do not interact with each other, $\hat{\mathrm{f}}^{\mathrm{KS}}$ named Kohn-Sham operator. A new *effective local potential* $\mathrm{V_S}$ is added to account for the electron-electron interaction with the Hamiltonian of the non-interacting system $\hat{\mathrm{H}}_{\mathrm{S}}$ has the form:

$$\hat{\mathrm{H}}_{\mathrm{S}} = -\frac{1}{2}\sum_{i}^{N}\nabla_i^2 + \sum_{i}^{N}\mathrm{V_S}(r_i), \tag{2.26}$$

where consequently no electron-electron term appears. A pseudo-wave function Θ_{S} is now constructed in a Hartree-Fock manner:

$$\Theta_{\mathrm{S}} = \frac{1}{\sqrt{N!}}\begin{vmatrix} \varphi_1(\boldsymbol{x}_1) & \cdots & \varphi_N(\boldsymbol{x}_1) \\ \vdots & \ddots & \vdots \\ \varphi_1(\boldsymbol{x}_N) & \cdots & \varphi_N(\boldsymbol{x}_N) \end{vmatrix}, \tag{2.27}$$

such that the density is exactly recovered from the Kohn-Sham orbitals φ_i

$$\rho_{\mathrm{S}}(\boldsymbol{r}) = \sum_{i}^{N}\sum_{s}|\varphi_i(\boldsymbol{r}, s)|^2 = \rho_0(\boldsymbol{r}). \tag{2.28}$$

The Kohn-Sham orbitals

As mentioned above the main idea of the Kohn-Sham Ansatz consists of finding a new way to more accurately determine the kinetic energy, calculating as most as possible of it exactly. The kinetic energy of the non-interacting system is described as in the true, interacting one with a expression equivalent to the one used within the Hartree-Fock theory (using KS orbitals instead of the HF ones 2.27)

$$\mathrm{T_S} = -\frac{1}{2}\sum_{i}^{N}\langle\varphi_i|\nabla^2|\varphi_i\rangle. \tag{2.29}$$

The non-interacting kinetic energy $\mathrm{T_S}$ does not carry all the kinetic energy $\mathrm{T} \neq \mathrm{T_S}$. The difference with the interacting system is included into a new functional named $\mathrm{E_{XC}}$ that contains all the non-classical interactions

$$\mathrm{E_{XC}}[\rho] = \big(\mathrm{T}[\rho] - \mathrm{T_S}[\rho]\big) + \big(\mathrm{E}_{ee}[\rho] - \mathrm{J}[\rho]\big) = \mathrm{T_C}[\rho] + \mathrm{E}_{ncl}[\rho]. \tag{2.30}$$

The *exchange-correlation functional* $\mathrm{E_{XC}}$ still remains unknown and the search for the exact one is the main challenge of DFT. It includes:

- effects of the self-interaction correction
- exchange (antisymmetry)
- correlation
- a portion belonging to the kinetic energy

After this the expression for the energy of the true, interacting system is written as follows:

$$\mathrm{E}[\rho(\boldsymbol{r})] = \mathrm{T_S}[\rho] + \mathrm{J}[\rho] + \mathrm{E_{XC}}[\rho] + \mathrm{E_{Ne}}[\rho], \tag{2.31}$$

where J is the Coulomb term, $\mathrm{T_S}$ the part of the kinetic energy exactly determined by the non-interacting system, $\mathrm{E_{XC}}$ the unknown non-classical exchange-correlation functional and the external potential that accounts for the nuclei-electron interaction $\mathrm{E_{Ne}}$.

The next step will be to find the proper orbitals for the non-interacting system. To that end we will expand Eq. 2.31 to:

$$\begin{aligned}\mathrm{E}[\rho(\boldsymbol{r})] = &-\frac{1}{2}\sum_{i}^{N}\langle\varphi_i|\nabla^2|\varphi_i\rangle + \\ &+\frac{1}{2}\sum_{i}^{N}\sum_{j}^{N}\int\int|\varphi_i(\boldsymbol{r}_1)|^2\frac{1}{r_{12}}|\varphi_j(\boldsymbol{r}_2)|^2 d\boldsymbol{r}_1 d\boldsymbol{r}_2 + \\ &+\mathrm{E_{XC}}[\rho(\boldsymbol{r})] - \sum_{i}^{N}\int\sum_{A}^{N}\frac{Z_A}{r_{1A}}|\varphi_i(\boldsymbol{r}_1)|^2 d\boldsymbol{r}_1.\end{aligned}$$

Note that the unknown exchange-correlation term cannot be given any explicit form.

LCAO Ansatz for the resolution of the Kohn-Sham Equations

By variationally minimizing the true energy expression 2.31 with respect to the KS single-particle orbitals, we get the following 1-electron equation

$$\varepsilon_i\varphi_i(\boldsymbol{r}_1) = \left(-\frac{1}{2}\nabla_1^2 + \left[\sum_{j}^{N}\int\frac{|\varphi_j(\boldsymbol{r}_2)|^2}{r_{12}}d\boldsymbol{r}_2 + \mathrm{V_{XC}}(\boldsymbol{r}_1) - \sum_{A}^{M}\frac{Z_A}{r_{1A}}\right]\right)\varphi_i(\boldsymbol{r}_1), \quad (2.32)$$

or

$$\varepsilon_i\varphi_i = \hat{\mathrm{f}}^{\mathrm{KS}}\varphi_i. \quad (2.33)$$

The set of KS orbitals, as within the Hartree-Fock context are expanded in terms of a finite basis set that does not provide the exact orbitals but approximates them. The larger the basis set the better the approximation but also the more expensive the calculation. For an infinite basis set every KS orbital will be exactly described.

Eq. 2.33, with the orbitals expanded as a linear combination of the basis set has to be solved. The Coulomb operator J and the exchange-correlation operator $\mathrm{E_{XC}}$ of Eq. 2.31 are dependent on the electron density ρ, which is function of the orbitals φ. However these orbitals are being searched in order to determine the electron density entering in that way in a *Self-Consistency problem* (Fig. 2.1).

A guessed initial density ρ_0 is introduced since it is needed to calculate the orbitals, that of course will not be the correct ones. The KS hamiltonian H_{KS} is found from the Coulomb (also called Hartree-Fock potential) and the exchange-correlation potentials. There are many different approaches to approximate this exchange-correlation potential as LDA, LSDA, GGA, meta-GGA... not discussed here. For a more detailed description of these approximations to $\mathrm{E_{XC}}$ functional the reader is referred to [18], [24] and [25]. When the KS hamiltonian, named $\hat{\mathrm{f}}^{\mathrm{KS}}$

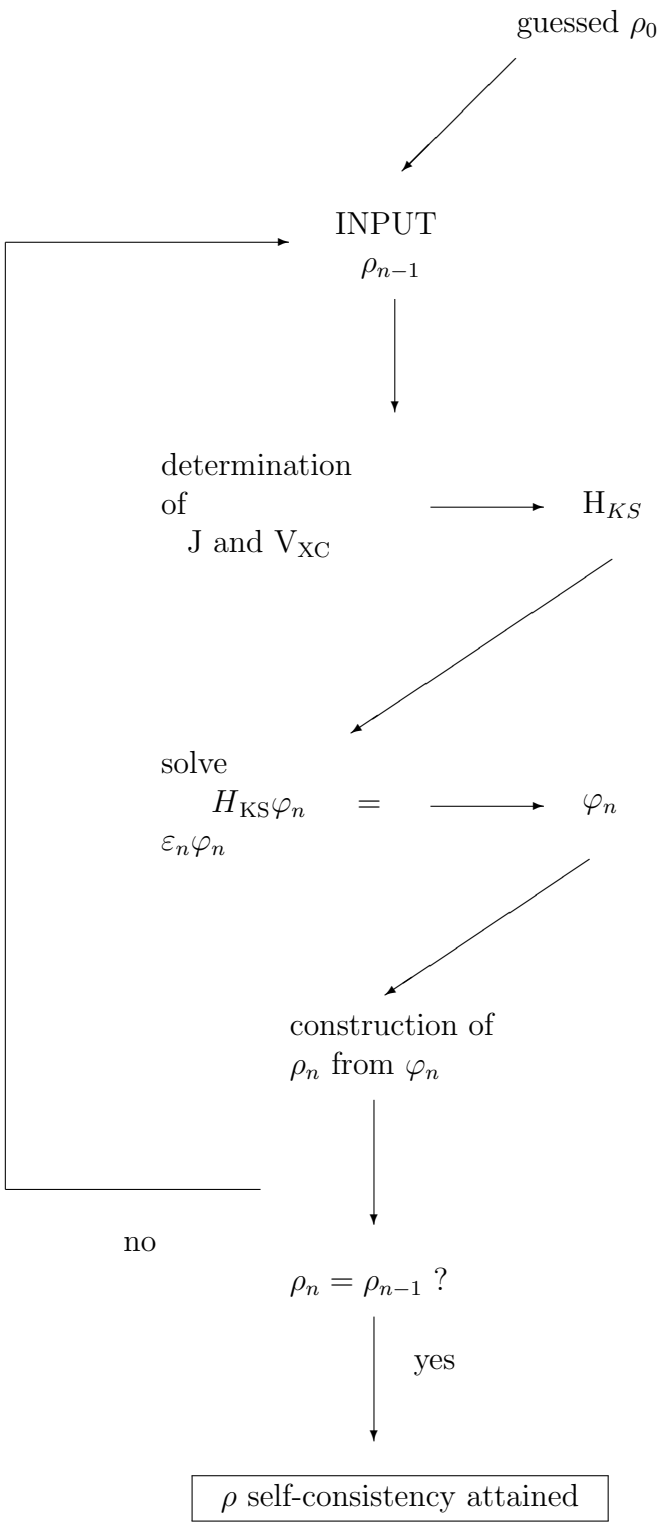

Figure 2.1.: Scheme of the iterative self-consistent procedure to solve the Kohn-Sham equations [23].

within the Kohn-Sham approach has been found, the secular equation (see Eq. 2.33) is solved yielding a set of orbitals φ_n. From these orbitals a new density ρ_n is obtained which will be different from the previous one ρ_{n-1}. Once we have arrived to a point where the difference between both densities is under a threshold the self-consistent loop is thought to be converged and the calculation comes to an end.

2.2.4. Electron Distribution and Density Matrices

We will include in this section just a brief selection of the ideas explained in [26]. For a discussion more in detail the reader is referred to the cited work.

Due to the increasingly improved computational facilities wave functions for chemical systems become so complicated that they provide no clear information of the electron distribution. Many chemical and physical properties of the system are inferred from this electron distribution and therefore information about it must be somehow extracted from the wave function. This relevant information is in fact contained in a few density functions normally easy to get a clear physical picture from.

The wave function of a one-electron system $\psi_A(\boldsymbol{x})$ is known as a spin orbital, meaning that it consists of a function termed *orbital* that describes the region of the space occupied by the electron $\phi_A(\boldsymbol{x})$, and by another function describing the spin of the electron $\sigma_A(s)$. s can be α —spin-up— for $s = +\frac{1}{2}$ or β —spin-down— for $s = -\frac{1}{2}$.

The wave function itself is not observable. Only from the square of this wave function, the *density function*, can be obtained some physical information:

$$\rho(\boldsymbol{x}) = |\psi_A(\boldsymbol{x})|^2. \tag{2.34}$$

It determines the probability of finding one electron in the volume element $d\boldsymbol{r}$ with spin between s and $s + \mathrm{d}s$. Decomposing the spin orbital it adopts the form:

$$\rho(\boldsymbol{x})\mathrm{d}\boldsymbol{x} = |\phi_A(\boldsymbol{r})|^2|\alpha(s)|^2\mathrm{d}\boldsymbol{r}\mathrm{d}s. \tag{2.35}$$

Summing over all spin possibilities —integrating over spin— we obtain the probability of finding the electron in the volume element $\mathrm{d}\boldsymbol{r}$ regardless of the spin.

The above equations can be generalized to the N electron case. The many-body wave function looks like $\Psi(\boldsymbol{x}_1, \boldsymbol{x}_2 \ldots \boldsymbol{x}_N)$ and the squared of it is the probability of finding electron 1 in $\mathrm{d}\boldsymbol{x}_1$, 2 in $\mathrm{d}\boldsymbol{x}_2$, ... and N in $\mathrm{d}\boldsymbol{x}_N$, simultaneously:

$$\Psi(\boldsymbol{x}_1, \boldsymbol{x}_2 \ldots \boldsymbol{x}_N)\Psi^*(\boldsymbol{x}_1, \boldsymbol{x}_2 \ldots \boldsymbol{x}_N)\mathrm{d}\boldsymbol{x}_1\mathrm{d}\boldsymbol{x}_2 \ldots \mathrm{d}\boldsymbol{x}_N. \tag{2.36}$$

Integrating over the space coordinates and spins of all electrons but one we get, due to the indistiguishable character of electrons, N-times the probability of finding one electron of any spin in $\mathrm{d}\boldsymbol{x}_1$ whereas the rest of the electrons may be anywhere in space. This quantity is known as the *electron density*[4]

[4] Strictly speaking it is a probability density but it is usually given the name electron density, since the electrons can be understood as "smeared out" within the volume element, with a certain density P.

$$\rho_1(\boldsymbol{r}_1) = \mathrm{N} \int \Psi(\boldsymbol{x}_1, \boldsymbol{x}_2 \ldots \boldsymbol{x}_N)\Psi^*(\boldsymbol{x}_1, \boldsymbol{x}_2 \ldots \boldsymbol{x}_N)\mathrm{d}s_1\mathrm{d}\boldsymbol{x}_2 \ldots \mathrm{d}\boldsymbol{x}_N. \tag{2.37}$$

The electron density is a non-negative quantity and also an observable —can be obtained by acting on the wave function with the corresponding operator— that integrates to the total number of electrons N and vanishes at infinity:

$$\int \rho(\boldsymbol{r})d\boldsymbol{r} = \mathrm{N}, \tag{2.38}$$

$$\rho(\boldsymbol{r} \to \infty) = 0. \tag{2.39}$$

Up to now only one particle has been considered but similar concepts, *mutatis mutandis* may be extended to higher number of particles. The pair function corresponds to a probability density for two electrons: the *electron pair density*

$$\rho_2(\boldsymbol{r}_1, \boldsymbol{r}_2) = \mathrm{N}(\mathrm{N}-1) \int |\Psi(\boldsymbol{x}_1, \boldsymbol{x}_2 \ldots \boldsymbol{x}_N)|^2\mathrm{d}s_1\mathrm{d}s_2\mathrm{d}\boldsymbol{x}_3 \ldots \mathrm{d}\boldsymbol{x}_N. \tag{2.40}$$

The electron pair density is defined as the probability of finding one electron within the volume element $d\boldsymbol{r}_1$ and simultaneously another one in $d\boldsymbol{r}_2$ whereas the remaining N−2 electrons are anywhere in space, regardless of spin.

How the motions of two electrons are correlated is described by the pair function. It is normalized to the total number of electron pairs that can be formed $\mathrm{N}(\mathrm{N}-1)$ and as the electron density is non-negative. For non-iteracting particles the probability of finding one particle at one point of the space and simultaneously another one at any other point, would be just the product of the individual probabilities:

$$\rho_2(\boldsymbol{x}_1, \boldsymbol{x}_2) = \frac{\mathrm{N}-1}{\mathrm{N}}\rho(\boldsymbol{x}_1)\rho(\boldsymbol{x}_2). \tag{2.41}$$

The term $(\mathrm{N}-1)/\mathrm{N}$ arises due to the indistiguishability of the electrons.

Density Matrices

It can be useful to slightly generalize the density functions from Eq. 2.37 and 2.40. For a 1-electron system, the expectation value of any operator F when the electron is located in the spin orbital ψ is given by

$$\langle F \rangle = \int \psi^*(\boldsymbol{x})F\psi(\boldsymbol{x})\mathrm{d}\boldsymbol{x}. \tag{2.42}$$

When F is a real operator that acts only on the right $\psi(\boldsymbol{x})$, $\psi^*(\boldsymbol{x})$ being unaffected by it. Hence the factors order matters and it cannot be expressed as

$$\langle F \rangle = \int F\psi^*(\boldsymbol{x})\psi(\boldsymbol{x})\mathrm{d}\boldsymbol{x}.$$

This can be solved by changing the name of the variables in ψ^* from $\boldsymbol{x}$ to $\boldsymbol{x}'$ making them immune to the action of F. The previous equation can now be expressed as

$$\langle F \rangle = \int_{\boldsymbol{x}'=\boldsymbol{x}} F\rho(\boldsymbol{x};\boldsymbol{x}')\mathrm{d}\boldsymbol{x}, \tag{2.43}$$

where the electron density from Eq. 2.37 is now generalized to the *non-diagonal reduced 1-density matrix*, which takes the form

$$\rho_1(\boldsymbol{r}_1;\boldsymbol{r}_1') = N\int \Psi(\boldsymbol{x}_1,\boldsymbol{x}_2\ldots\boldsymbol{x}_N)\Psi^*(\boldsymbol{x}_1',\boldsymbol{x}_2\ldots\boldsymbol{x}_N)\mathrm{d}s_1\mathrm{d}\boldsymbol{x}_2\ldots\mathrm{d}\boldsymbol{x}_N. \tag{2.44}$$

The prime keeps its special character during the action of the operator F and loses it just before the integration. In that way F acts only on the unprimed wave function while the subsequent integration affects all terms.

Of course the same applies to the two-electron case, where the *non-diagonal reduced 2-density matrix*, has the following expression.

$$\rho_2(\boldsymbol{r}_1,\boldsymbol{r}_2;\boldsymbol{r}_1',\boldsymbol{r}_2') = \mathrm{N(N-1)}\int \Psi(\boldsymbol{x}_1,\boldsymbol{x}_2\ldots\boldsymbol{x}_N)\Psi(\boldsymbol{x}_1',\boldsymbol{x}_2'\ldots\boldsymbol{x}_N)\mathrm{d}s_1\mathrm{d}s_2\mathrm{d}\boldsymbol{x}_3\ldots\mathrm{d}\boldsymbol{x}_N. \tag{2.45}$$

Both the electron density and the electron pair density are recovered as the diagonal part of the corresponding density matrices

$$\rho_1(\boldsymbol{r}) = \rho_1(\boldsymbol{r}_1;\boldsymbol{r}_1), \qquad \rho_2(\boldsymbol{r}_1,\boldsymbol{r}_2) = \rho_2(\boldsymbol{r}_1,\boldsymbol{r}_2;\boldsymbol{r}_1,\boldsymbol{r}_2).$$

The information about the correlation of electronic motion is understood to be contained in the electron pair density function. This electron correlation can be of two distinct types:

- ***Fermi or exchange correlation:*** In Eq. 2.45 is defined the generalized reduced density matrix for two electrons, where the primed coordinates are not integrated. The antisymmetry of the wave function established by the Pauli principle states that interchanging the positions of two electrons ($\boldsymbol{x}_1$ and $\boldsymbol{x}_2$) for example, will cause $\rho_2(\boldsymbol{r}_1,\boldsymbol{r}_2;\boldsymbol{r}_1',\boldsymbol{r}_2')$ to have its sign changed

  $$\rho_2(\boldsymbol{r}_1,\boldsymbol{r}_2;\boldsymbol{r}_1',\boldsymbol{r}_2') = -\rho_2(\boldsymbol{r}_2,\boldsymbol{r}_1;\boldsymbol{r}_1',\boldsymbol{r}_2')$$

  In the specific case where we take the diagonal part of this matrix ($\boldsymbol{x}_1 = \boldsymbol{x}_1'$ and $\boldsymbol{x}_2 = \boldsymbol{x}_2'$, cf. section 2.2.4) we recover the pair density $\rho_2(\boldsymbol{r}_1,\boldsymbol{r}_2)$ as

defined in Eq. 2.40. For the special case in which both electrons are sharing not only the same position but also the same spin $\boldsymbol{x}_1 = \boldsymbol{x}_2$,

$$\rho_2(\boldsymbol{r}_1, \boldsymbol{r}_1) = -\rho_2(\boldsymbol{r}_1, \boldsymbol{r}_1). \tag{2.46}$$

which is the probability that both electrons are identical and occupy exactly the same location, relation that is satisfied solely by the condition $\rho_2(\boldsymbol{r}_1, \boldsymbol{r}_1) = 0$. This is the exchange correlation which is considered by the HF approach as a consequence of the antisymmetry of a Slater determinant, but has nothing to do with the correlation included in the correlation energy E_C^{HF} in the previous chapter (see Eq. 2.18).

- ***Coulomb correlation:*** However electrons of opposite spin do not suffer the Fermi correlation but are subject to an electrostatic interaction coming from the term $1/r_{ij}$ in Eq. 2.4. There is a repulsion force that applies to all electrons —no matter the spin— due to their charge that prevents them to approximate to each other. This correlation between the motions of the electrons due to their charge is the Coulomb correlation or simply the electron correlation and is not treated at all by the HF approach.

  In that case, the expansion of the determinants, whereas for the parallel spin situation the Pauli principle is fulfilled, as already mentioned $\rho_2^{HF,\sigma_1=\sigma_2}(\boldsymbol{r}_1, \boldsymbol{r}_2) = 0$. But if the electrons have opposite spin the pair probability equals the product of the individual probabilities and does not take into account the electron correlation $\rho_2^{HF,\sigma_1\neq\sigma_2}(\boldsymbol{r}_1, \boldsymbol{r}_2) = \rho_1(\boldsymbol{r}_1)\rho_1(\boldsymbol{r}_2)$.

The Fermi and Coulomb correlation can now be included into a correlation factor $f(\boldsymbol{x}_1; \boldsymbol{x}_2)$, a term that allows the correlation of electronic motion to be separed from the non-interacting situation, yielding an alternative definition of the pair density expression, which is as follows:

$$\rho_2(\boldsymbol{x}_1, \boldsymbol{x}_2) = \rho(\boldsymbol{x}_1)\rho(\boldsymbol{x}_2)\big[1 + f(\boldsymbol{x}_1; \boldsymbol{x}_2)\big]. \tag{2.47}$$

This correlation factor will vanish in case the electrons do not see each other.

A new function can now be defined: the *conditional probability* $\Omega(\boldsymbol{x}_1; \boldsymbol{x}_2)$. As its name indicates, it describes the probability of finding one electron at position $\boldsymbol{x}_2$ subject to the condition that another one is already at $\boldsymbol{x}_1$

$$\Omega(\boldsymbol{x}_1; \boldsymbol{x}_2) = \frac{\rho_2(\boldsymbol{x}_1, \boldsymbol{x}_2)}{\rho_1(\boldsymbol{x}_1)}. \tag{2.48}$$

This conditional density integrates to N-1, the total number of electrons except the reference electron at $\boldsymbol{x}_1$. If we make the difference between the conditional density and the uncorrelated probability of finding an electron at $\boldsymbol{x}_2$, we get the *exchange-correlation hole*

$$\mathrm{h_{XC}}(\boldsymbol{x}_1;\boldsymbol{x}_2) = \frac{\rho_2(\boldsymbol{x}_1,\boldsymbol{x}_2)}{\rho_1(\boldsymbol{x}_1)} - \rho(\boldsymbol{x}_2). \tag{2.49}$$

The function known as exchange-correlation hole describes the change in the conditional probability provoqued by the correction for self interaction, Fermi and Coulomb correlation in comparison to the totally uncorrelated situation. This quantity is called a hole since it normally caused depletion of electron density at $\boldsymbol{x}_2$ compared to the independent particle situation. It can be understood as a hole the electron creates around itself where no other electron is likely to be found. Since the pair density integrates to N-1 and the density at $\boldsymbol{x}_2$ to N, the exchange-correlation hole integrates to -1. In other words, it contains exactly the charge of one electron

$$\int \mathrm{h_{XC}}(\boldsymbol{x}_1;\boldsymbol{x}_2)\mathrm{d}\boldsymbol{x}_2 = -1.$$

There are no many-body interactions among electrons in the Coulomb approximation. As a consequence there is no need to consider distribution functions of higher number of electrons than the pair function ρ_2.

2.3. Chemical bond descriptors in real space

2.3.1. Quantum Theory of Atoms In Molecules QTAIM

Many chemical concepts introduced on an empirical basis can be assigned a physical explanation through the QTAIM theory. Taking the electron density ρ as the central property QTAIM is able to confer physical meaning, via the topology of the electron density, to basic chemical concepts as bonds or atoms. A full, authoritative account of the theory may be found in [3] and [27].

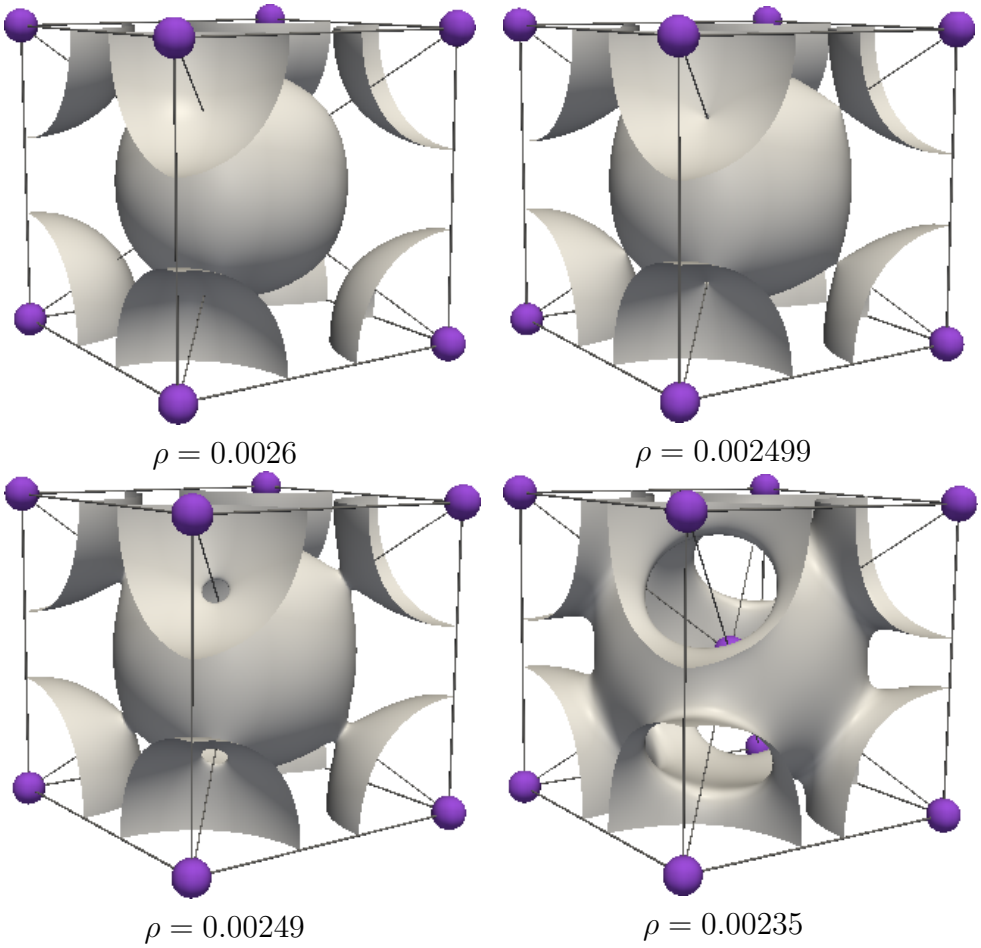

Figure 2.2.: Progression of the electron density isosurface for K *bcc* at four different $[\rho] = electronsbohr^{-3}$ values.

The electron density ρ forms a uniform distribution around the atoms of the system. In Fig. 2.2 can be visualize a density isosurface where all points have the same electron density value. Four different figures can be observed for four different density values of *bcc* K, specified in the figure.

If the isosurface attains higher values than ≈ 0.0025 each atom is surrounded by a spherical shell that corresponds to the atomic basins. Each one of these

domains is irreducible and includes only one critical point (see below). But as the isovalues are reduced and approximate to 0.0025 the sphericity around the atoms is lost and the spheres come together establishing contact in one point, termed *critical point* (in 2.2 see figure with $\rho = 0.002499$). When isovalues are further reduced the single spheres form a single one as can be seen in the last figure $\rho = 0.00235$ which forms a single domain including more than one attractor. It can not be assigned to only one atom and consequently loses its topological meaning.

Critical Points

The critical points (CP) of ρ are points in real space where the electron density gradient vanishes $\vec{\nabla}\rho(\boldsymbol{r}) = (0, 0, 0)$ and mark special positions in space. CPs can be local minima, maxima or saddle points of the electron density. The differentiation among the different sorts of critical points can be achieved by means of the associated hessian matrix $H(\rho(\boldsymbol{r}))$, which is a real, symmetric 3×3 matrix formed by the pure and mixed second derivatives of the electron density:

$$H(\vec{\boldsymbol{r}}) = \begin{pmatrix} \frac{\partial^2}{\partial x^2} & \frac{\partial^2}{\partial x \partial y} & \frac{\partial^2}{\partial x \partial z} \\ \frac{\partial^2}{\partial y \partial x} & \frac{\partial^2}{\partial y^2} & \frac{\partial^2}{\partial y \partial z} \\ \frac{\partial^2}{\partial z \partial x} & \frac{\partial^2}{\partial z \partial y} & \frac{\partial^2}{\partial z^2} \end{pmatrix}$$

Diagonalization of the hessian matrix $H\rho(\boldsymbol{r})$ yields the eigenvalues h_{xx}, h_{yy}, h_{zz}. That allows us to classify a critical point by its 'rank' and 'signature'. The *rank* is defined as the number of non-zero eigenvalues of the hessian matrix; in other words, the maximum number of rows (or columns) that are linearly independent vectors. The *signature* is defined as $s = \sum \frac{h_{ii}}{|h_{ii}|}$. In case one or more hessian eigenvalues are equal to zero, i.e., one or more rows (columns) can be expressed as a linear combination of the others, the point is a degenerate critical point. However we will only disscuss here the "nondegenerate critical points", which can be of four types:

Minimum also known as repelor or $(3, +3)$ critical point, if all principal curvatures of the electron density are positive. They can also be given the name Cage Critical Points (CCP).

Maximum attractor or $(3, -3)$ critical point, for cases with all curvatures being negative.

Saddle point two situations can occur:

Bond critical point (BCP) or $(3, -1)$ critical point, for hessian matrices with one principal curvature positive and two negative.

Ring critical point (RCP) or $(3, +1)$ critical point, in case one principal curvature negative and two positive.

In order to obtain a well-behaved quantum-mechanical description of an open region of a quantum system, it must be bounded in any way and enclose a finite volume [11]. Eq. 2.50 will be the condition neccessary to limit the extension of the non-overlapping regions defining a basin:

$$\nabla\rho(\boldsymbol{r}_s) \cdot \mathbf{n} = 0, \tag{2.50}$$

where $\mathbf{n}$ is the vector normal to the boundary surface, namely the exterior normal and $\boldsymbol{r}_s$ indicates that the electron density is evaluated at each point of the surface.

A basin is then a region of space where all gradient paths (trajectories) of a chosen scalar field such as electron density terminate at the same ω-*limit* that is a maximum. In general, each of these basins contains only one nucleus which corresponds to the aforementioned maxima or attractors: a basin usually represents an atom. Otherwise the basin is associated with so called non-nuclear attractor [28]. Every of the basins of a system is bounded by zero-flux surfaces defined by the condition described in Eq. 2.50, which are trajectories terminating at a ω-*limit* that now is a saddle-point.

The partition of the space can however be done according to scalar fields other than the electron density. The Electron Localizability Indicator ELI $\Upsilon_D^\sigma(\boldsymbol{r})$ will be explained in the next section 2.3.2. It can as well be used to partition the space into basins (localization domains) that have dissimilar interpretations to the basins defined according to the QTAIM.

2.3.2. Restricted Space Partitioning

> A ω-restricted partitioning (ωRSP) of the space consists of a subdivision of the system volume into non-overlapping space-filling regions of maximum compactness in such a way that the integral of the control property over any region yields ω.

One strategy to extract information about a system is the examination of a certain property over samples characterized by the same (chosen) quantity, thus allowing the sampled results to be compared. The restricted space partitioning into extremely small regions, namely the samples over the system under study for us, is done according to a chosen quality ω known as *control* property. This results in a ω-restricted division of the space into regions named μ_i of volume V_i centered at a chosen position $\boldsymbol{a}_i$. The control property regulates the space partitioning and hence determines the regions volume by satisfying the condition that a fixed ω value will be enclosed within them. Each region will attain such volume that this condition, the ω restriction, is fulfilled. The *sampling* property is then evaluated at each of the region's center $\boldsymbol{a}_i$.

Although the shape of the sample regions can in principle freely adopt any shape, the partitioning of the space is not arbitrarily done (Fig. 2.3). The system is divided into non-overlaping, space-filling regions complying the restriction ω and being as compact as possible.

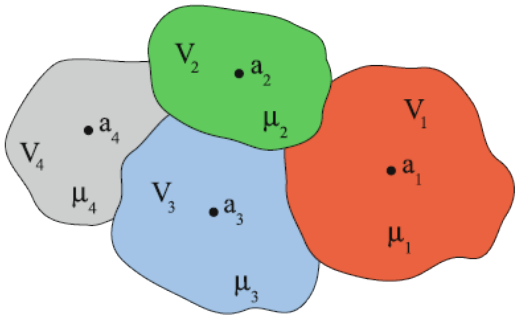

Figure 2.3.: Schematic representations of the result of a ω-restricted partition of the space. Every region μ_i is centered at $\boldsymbol{a}_i$ and has a volume V_i imposed by the ω-restriction and arbitrary shape.

In spite of being the most compact isolated region a sphere, the shape of the regions cannot be spherical when constricted to the conditions we just mentioned. They will rather adapt the most compact form given that neighbouring regions present maximal compactness as well. Nevertheless, the shape the ω-partitioned regions can adopt is still infinite. A simplified scheme of the way from the base, the restricted population approach, to the top of the ω-restricted partitioning can be found below.

The control function f_c: the ω-Restricted Space Partitioning

The number of sampling regions is determined by the ω values and the integral of the control function f_c over the whole system $F_c = \int f_c(\boldsymbol{r})d\boldsymbol{r}$. Among the different possibilites we could have depending on the value of the integral F_c, we will only be interested in the situation in which the integral of the control funcion over the whole system yields a non-zero real value $F_c \neq 0$ [5]. In that case, there will be a uniquely given finite $\kappa = F_c/\omega$ number of regions for any real restriction $\omega \neq 0$.

In that case, when choosing infinitesimally small restrictions (infinitesimally small meaning small enough) the density of the regions (number of regions per volume unit) does not vary significantly for all the possible ways of dividing the space. It is possible to use small enough ω restriction values in such a way that choosing any of the possible manners of partitioning the system (slightly shifting the center $\boldsymbol{a}_i$) will not increase the number of regions κ (density of sample regions). From now on we will refer to the very small regions as *micro-cells*.

Restricted population approach:
Space division into mutually-exclusive space-filling regions
↳ **Compact regions:**
Locality of the examined effects
↳ **Integral of ω property over μ_i = <u>constant</u>:**
ω-restricted partitioning of the space
⇓
Partition of the space into compact, mutually exclusive and space-filling micro-cells *with ω-dependent variable volumes*

Due to the choice of extremely small sampling regions the system presents certain properties. Additionally, the *micro-cells* being so small makes it possible to approximate the integrals of chosen functions over such regions by polynomials based on the first non-vanishing term of the corresponding Taylor expansion (the approximation of the sampling function integrals over the *micro-cells* by a Taylor

[5] For a deeper disscussion see [29].

expansion will be discussed later on).

Let us consider as control function a one-particle property: the electron density, $\rho_1(\boldsymbol{r})$ derived from generalized density matrices as explained in chapter 2.2.4. Integration of the electron density $\rho_1(\boldsymbol{r})$ over the whole space yields the total number of electrons N in the system. On the other hand, the integral of this control function over any of the non-overlapping space filling regions μ_i into which the system is partitioned will yield the fixed electronic charge $q = \omega$ within this region μ_i:

$$q = \int_{\mu_i} \rho_1(\boldsymbol{r}) d\boldsymbol{r} = \omega \ . \tag{2.51}$$

The system is hence partitioned into $\kappa = N/q$ regions. Given that those regions are *micro-cells* in the sense explained before, the charge within it can be approximated by $q \approx \rho_1(\boldsymbol{a}_i)V_i$. The volume of the *micro-cell* V_i is hence inversely proportional to the electron density, which is valid for any control function normalised to $F_c = \int f_c(\boldsymbol{r})d\boldsymbol{r}$:

$$V_i \approx \omega / f_c(\boldsymbol{a}_i) \qquad F_c = \kappa\omega \ . \tag{2.52}$$

For n coordinates it is not so easy and the number of *micro-cells* κ cannot be found in the same way. Let us consider now a partition of the space using a two-particle quantity, the electron pair density $\rho_2(\boldsymbol{r}_1, \boldsymbol{r}_2)$ (Eq. 2.40), as control function. Each region μ_i encloses now a fixed number of electron pairs D_i. The general expression for a control function f_c of n coordinates:

$$\omega = \int_{\mu_i} d\boldsymbol{r}_1 \ldots \int_{\mu_i} f_c(\boldsymbol{r}_1, \ldots, \boldsymbol{r}_n) d\boldsymbol{r}_n \ , \tag{2.53}$$

becomes now:

$$D = \int_{\mu_i} d\boldsymbol{r}_1 \int_{\mu_i} \rho_2(\boldsymbol{r}_1, \boldsymbol{r}_2) d\boldsymbol{r}_2 \ . \tag{2.54}$$

Here the number κ of *micro-cells* μ_i for a given restriction ω follows $\kappa\omega \leq N(N-1)/2$, satisfying that the total number of electron pairs in the system must be equal or higher than the number of electron pairs in all the *micro-cells*.

The sampling function f_s: Restricted Populations

The first part for the restricted space partitioning is already achieved: the control function determines the decomposition of the space into sample regions over which the property of interest will be evaluated.

As already mentioned, the m-th order spinless reduced density matrix is obtained integrating the N-th order density matrix over the coordinates of $(N-m)$

electrons over the whole space and summing over both α and β spins.

For operators fulfilling a few conditions (they must be spin-free and one- or two-electron operators), the reduced 2-matrix $\gamma^{(2)}(\boldsymbol{r}'_1\boldsymbol{r}'_2, \boldsymbol{r}_1\boldsymbol{r}_2)$ carries enough information to find the expectation value of such operators.

Let us consider a sampling property whose expectation value is given by the operator $\hat{A}$, satisfying the above conditions, acting on the wave function of the system ψ integrated over all space:

$$\left\langle \hat{A} \right\rangle = \int \Psi^* \hat{A} \Psi dV \ . \tag{2.55}$$

$\hat{A}$ being a single-particle operator the previous expression can be reduced to a sum over all the κ *micro-cells* (having the spin integrated out):

$$\left\langle \hat{A} \right\rangle = \int \hat{A}\gamma^{(1)}(\boldsymbol{r}';\boldsymbol{r})d\boldsymbol{r} = \sum_{i=1}^{\kappa} \int_{\mu_i} \hat{A}\gamma^{(1)}(\boldsymbol{r}';\boldsymbol{r})d\boldsymbol{r} \ . \tag{2.56}$$

The operator $\hat{A}$ acting on the 1-matrix yields a function that we call here the sampling function f_s. For a single-particle operator the sampling function will take the form:

$$f_s(\boldsymbol{r}) = \hat{A}\gamma^{(1)}(\boldsymbol{r}';\boldsymbol{r})|_{r'\to r}$$

while for two-particle operator

$$f_s(\boldsymbol{r}_1, \boldsymbol{r}_2) = \hat{A}\gamma^{(2)}(\boldsymbol{r}'_1, \boldsymbol{r}'_2; \boldsymbol{r}_1, \boldsymbol{r}_2)|_{r'\to r}$$

Evaluation of the expectation value $A = \left\langle \hat{A} \right\rangle$ involves the equating of the primed and unprimed coordinates, resulting in a function which has to be further integrated over the whole space. The resulting expectation value is the electron density $\rho_1(\boldsymbol{r})$, which corresponds to the diagonal part of the 1-matrix $\gamma^{(1)}(\boldsymbol{r}';\boldsymbol{r})$, is a particular case of a sampling property for single-particle operator. The integral of $\rho_1(\boldsymbol{r})$ over the whole space yields the total number of electrons in the system, i.e., is normalised to the number of electrons N. Integration over a *micro-cell* μ_i yields the charge of that region q_i fulfilling that $\sum q_i = N$.

Electron pair density $\rho_2(\boldsymbol{r}_1, \boldsymbol{r}_2)$ is the expectation value for the operator $\left\langle \hat{A} \right\rangle$ being a two-particle operator and corresponds to the diagonal part of the 2-matrix $\gamma^{(2)}(\boldsymbol{r}'_1, \boldsymbol{r}'_2; \boldsymbol{r}_1, \boldsymbol{r}_2)$, can be chosen as sampling property as well. Equivalently, it is normalised to the total number of electron pairs $N(N-1)/2$. However now the sum of the electron pair population in every *micro-cell* μ_i does not yield the total number of electron pairs in the system, since in order to get that also the electron pairs D_{ij} shared by two regions (region pairs) μ_i and μ_j must be considered.

In both cases, using first- or second-order electron densities as sample function f_s (and the same would apply for n-th order electron densities) we obtain a distribution of the electron populations $\{q_i\}$ and of the electron pair populations $\{D_i\}$,

respectively, for each region μ_i. The applied restriction will give the name to the distribution of values resulting from integrating f_s. In that way, integration of f_s over regions restricted according to an ωRSP are named ω-restricted populations.

Electron Localizability Indicator

A N-electron system is described by the wavefunction $\Psi(\boldsymbol{x}_1\boldsymbol{x}_2\cdots\boldsymbol{x}_N)$ with $\boldsymbol{x}_i = (\boldsymbol{r}_i, \sigma_i)$ being the position $\boldsymbol{r}_i$ and spin σ_i coordinates, respectively, of electron i. The information about the chemical bonding within such a system is carried by the N-matrix $\Gamma^{(n)}$. Since the energy can be found from 1 and 2-particle operators, we can assume that in the 2-matrix $\Gamma^{(2)}$ is contained a relevant part of this chemical information.

From this wavefunction 1 and 2-spinless density matrices can be found:

$$\rho_1(\boldsymbol{r}_1'|\boldsymbol{r}_1) = N \int d\sigma_1 \int d\boldsymbol{x}_2 \cdots \int d\boldsymbol{x}_N \Psi^*(\boldsymbol{x}_1'\boldsymbol{x}_2\cdots\boldsymbol{x}_N)\Psi(\boldsymbol{x}_1\boldsymbol{x}_2\cdots\boldsymbol{x}_N) \ , \quad (2.57)$$

$$\rho_2(\boldsymbol{r}_1'\boldsymbol{r}_2'|\boldsymbol{r}_1\boldsymbol{r}_2) = \binom{N}{2} \int d\sigma_1 \int d\sigma_2 \int d\boldsymbol{x}_3 \cdots \int d\boldsymbol{x}_N \Psi^*(\boldsymbol{x}_1'\boldsymbol{x}_2'\cdots\boldsymbol{x}_N)\Psi(\boldsymbol{x}_1\boldsymbol{x}_2\cdots\boldsymbol{x}_N) \ . \quad (2.58)$$

The elements in the main diagonal of these density matrices are the electron density and electron pair density, respectively, as previously described in section 2.3.2:

$$\rho_1(\boldsymbol{r}_1) = \rho_1(\boldsymbol{r}_1|\boldsymbol{r}_1) \ , \quad (2.59)$$

$$\rho_2(\boldsymbol{r}_1\boldsymbol{r}_2) = \rho_2(\boldsymbol{r}_1\boldsymbol{r}_2|\boldsymbol{r}_1\boldsymbol{r}_2) \ . \quad (2.60)$$

Since the 1-matrix was spinless the electron density is written as a sum of the two spin components, that are probability densities of finding one electron with the corresponding spin in real space:

$$\rho(\boldsymbol{r}_1) = \rho_\alpha(\boldsymbol{r}_1) + \rho_\beta(\boldsymbol{r}_1) \ , \quad (2.61)$$

which integrated becomes $N = N_\alpha + N_\beta$. α and β refer to up and down spin respectively. Similarly, the electron pair density is expressed as a sum of four components, each one being now the probability density of finding two electrons with the corresponding spin in position space:

$$\rho_2(\boldsymbol{r}_1, \boldsymbol{r}_2) = \rho_2^{\alpha\alpha}(\boldsymbol{r}_1, \boldsymbol{r}_2) + \rho_2^{\beta\beta}(\boldsymbol{r}_1, \boldsymbol{r}_2) + \rho_2^{\alpha\beta}(\boldsymbol{r}_1, \boldsymbol{r}_2) + \rho_2^{\beta\alpha}(\boldsymbol{r}_1, \boldsymbol{r}_2) \ . \quad (2.62)$$

According to Eq. 2.51 the integration of the σ-spin electron density $\rho(\boldsymbol{r}_1)$ over the region μ_i yields the σ-spin electron population q_σ, i.e., the charge within this region. In a similar way the integration of the same-spin electron pair density $\rho_2^{\sigma\sigma}(\boldsymbol{r}_1, \boldsymbol{r}_2)$ over the region μ_i yields the same-spin pair population $D_2^{\sigma\sigma}(\mu_i)$ (Eq. 2.54), i.e., the average number of same-spin electron pairs within the region.

The volumes of the regions enclose now a fixed number of same-spin electron pairs:

$$D_2^{\sigma\sigma}(\mu_i) = \int_{\mu_i} d\boldsymbol{r}_1 \int_{\mu_i} \rho_2(\boldsymbol{r}_1, \boldsymbol{r}_2) d\boldsymbol{r}_2 = const. \tag{2.63}$$

The sampling function is now the average number of σ-spin electrons (charge) which is evaluated integrating the electron density over the region μ_i. This functional is named the $D_2^{\sigma\sigma}$-restricted electron population $Q_i^{\sigma\sigma}(\mu_i)$ [6]:

$$Q_i^{\sigma}(\mu_i) = \int_{\mu_i} \rho_\sigma(\boldsymbol{r}) d\boldsymbol{r} \ . \tag{2.64}$$

The evaluation of these integrals over pair density can be approximated and hence simplified by the Taylor expansion of the σ-spin pair density around an arbitrary point $\boldsymbol{a}_1$ inside the region μ_i [7]. Due to the Pauli exclusion principle and the cusp condition, the first nonvanishing term of the Taylor expansion is the Fermi hole curvature at the position $\boldsymbol{r}_1$. The same-spin pair density is hereby approximated as:

$$D_2^{\sigma\sigma}(\mu_i) \approx \frac{1}{2} \int \int_{\mu_i} (\boldsymbol{s} \cdot \nabla_{\boldsymbol{r}_2})^2 \rho_2^{\sigma\sigma}(\boldsymbol{r}_1, \boldsymbol{r}_2)\big|_{\boldsymbol{r} \to \boldsymbol{a}} d\boldsymbol{r}_1 d\boldsymbol{r}_2 \ , \tag{2.65}$$

where $\boldsymbol{s} = \boldsymbol{r}_2 - \boldsymbol{r}_1$ but the operator $\nabla^2_{\boldsymbol{r}_2}$ acts only on the coordinate $\boldsymbol{r}_2$:

$$\frac{1}{2}(\boldsymbol{s} \cdot \nabla_{\boldsymbol{r}_2})^2 = \frac{1}{2} \sum_{i,j}^{x,y,z} \boldsymbol{s}_i \boldsymbol{s}_j \frac{\partial^2}{\partial i_2 \partial j_2} \ . \tag{2.66}$$

$\boldsymbol{s}_i = (r_2 - r_1)_i = (x_2 - x_1, y_2 - r_1, z_2 - z_1)_i$ and similarly for $\boldsymbol{s}_j$. As this expansion around the point $\boldsymbol{r}_1$ results in an new $\boldsymbol{r}_1$-dependent function which must be integrated, again a Taylor expansion can be applied, now around the point $\boldsymbol{a}_i$. After the second expansion the number of same-spin electron pairs can be approximated by:

$$D_i^{\sigma\sigma} \approx \frac{1}{12} V_i^{8/3} g(\boldsymbol{a}_i) \ . \tag{2.67}$$

[6] Note that the capital letter $Q^{\sigma\sigma}$ designates the charge as a sampling function in a $D_2^{\sigma\sigma}$-restricted population, whereas q_σ refers to the charge as the control function in a q_σ-restricted analysis.

[7] Giving each region a center serves as a way to differentiate the regions, that can be distinguished by the index a.

V_i is the volume of the *micro-cell* μ_i and $g(\boldsymbol{a}_i)$ the Fermi-hole curvature at the *micro-cell* center $\boldsymbol{a}_i$ [30].

$$g(\boldsymbol{a}_i) = \sum_{i<j}^{\sigma}\sum_{k<l}^{\sigma} P_{ij,kl}\left[\phi_i(\boldsymbol{a}_i)\nabla\phi_j(\boldsymbol{a}_i) - \phi_j(\boldsymbol{a}_i)\nabla\phi_i(\boldsymbol{a}_i)\right] \times \left[\phi_k(\boldsymbol{a}_i)\nabla\phi_l(\boldsymbol{a}_i) - \phi_l(\boldsymbol{a}_i)\nabla\phi_k(\boldsymbol{a}_i)\right] . \tag{2.68}$$

Given that we have selected sufficiently small regions the volume occupied by the fixed number of same-spin pairs can be obtained from the expression:

$$V_i \approx \left[\frac{12D^{\sigma\sigma}}{g(\boldsymbol{a}_i)}\right]^{3/8} \tag{2.69}$$

Since the volumes of the regions μ_i are very small, the $D^{\sigma\sigma}$-restricted population Q_i^{σ}, the σ-spin charge enclosed by the region can be approximated by the product between the σ-spin electron density and the region volume:

$$Q_i^{\sigma} \approx \rho_{\sigma}(\boldsymbol{a}_i)V_i = \rho_{\sigma}(\boldsymbol{a}_i)\left[\frac{12D^{\sigma\sigma}}{g(\boldsymbol{a}_i)}\right]^{3/8} . \tag{2.70}$$

If the dependence on $D^{\sigma\sigma}$ is removed the ELI-D expression is obtained:

$$\Upsilon_D^{\sigma}(\boldsymbol{a}_i) = \frac{Q_i^{\sigma}}{(D^{\sigma\sigma})^{3/8}} \approx \rho_{\sigma}(\boldsymbol{a}_i)\frac{V_i}{(D^{\sigma\sigma})^{3/8}} = \rho_{\sigma}(\boldsymbol{a}_i)\tilde{V}_D(\boldsymbol{a}_i) . \tag{2.71}$$

ELI-D is then proportional to the average number of electrons (charge) given by Q_i^{σ} that is needed to form the fixed fraction of a σ-spin electron pair $D^{\sigma\sigma}$. The rescaled volume $\tilde{V}_D(\boldsymbol{a}_i)$ is the pair-volume function. Sampling the chosen property (charge for D-restricted population) over the *micro-cells* yields a discrete distribution of values. If the restriction $D^{\sigma\sigma}$ is taken infinitesimally small the discrete distribution is so dense that can be regarded as continuous

$$\Upsilon_D^{\sigma}(\boldsymbol{a}_i)\big|_{D_{\sigma\sigma}\to 0} \to \Upsilon_D^{\sigma}(\boldsymbol{r}) , \tag{2.72}$$

and $\Upsilon_D^{\sigma}(\boldsymbol{a}_i)$ can be expressed as:

$$\Upsilon_D^{\sigma}(\boldsymbol{r}) = \rho(\boldsymbol{r})\tilde{V}_D(\boldsymbol{r}) = \left(\frac{12}{g(\boldsymbol{r})}\right)^{3/8} . \tag{2.73}$$

Space partitioning using ELI-D

As was already mentioned the relevant information to understand the chemical bonding is contained in the Pauli principle, as stated by the valence-shell electron-

pair repulsion (VSEPR) theory [31]. The analysis of the quantum-mechanical functions related to the Pauli exclusion principle such as the electron density or the ELI-D are consequently a main objective. The differential topological analysis of these local scalar functions is a well-established mathematical approach that allows inspection of the former functions [32]. This topological anaylisis can be interpreted by means of the critical points that were already described in section 2.3.

When these singularities are searched using gradient inspection techniques for ELI-D a bunch of critical points appear. The local maxima define "localization domains" that can be bonding, non-bonding and core which are the three types of basins that can be defined using two-particle quantities such as ELF [33] or ELI-D.

The localization domains can be of two types depending on whether they are encapsulating one or more critical points (CP) (see section 2.3 for explanation of CP). If they encapsulate one critical point they are called *irreducible* and varying the isovalue that surrounds the region induces deformation in the localization domains but does not alter its topological type though. A partition of the space into irreducible domains can be seen in Fig. 2.4c where the localization domains around the central Cl atom cannot be further partitioned, they keep their topological type. If the isovalue is increase they just disappear 2.4d. Nevertheless, if they embrace more than one CP, now named *reducible* localization domains, tuning of the ELI-D isovalues will cause bifurcation to occur for critical values of the quantity (ELI-D in our case). A bifurcation causes the break of the localization domain into several smaller localization domains containing fewer CPs until a irreducible one is found [32]. That is what we can observe in Fig. 3.3 where when increasing the isovalue the big reducible localization domain in 2.4a breaks into also reducible domains but containing less CPs (Fig. 2.4b). Finally fifurcation into irreducible domains causes a split into the 6 different irreducible localization domains of Fig. 2.4c.

Core critical points (attractors are normally assigned to nuclei) are located around the atomic nuclei, whereas *bonding* CPs (saddle points correspond to bonding critical point BCP) lie inbetween characterizing the shared-electron interactions. The number of bond attractors is related to the bond multiplicity. *Non-bonding* CPs are assigned to lone pairs. The regions surrounded by an isosurface are called a basin.

All the basins corresponding to critical points closer to the nucleus more than a tabulated distance are assigned to the same basin, since all of them are firmly linked to the nucleus and are not chemically active. These basins are merged together into a superbasin that represents the atomic core. Irreducible localization domains, i.e., each of them enclosing only one CP, corresponding to bonding CPs (saddle points) are bonding basins that represent the valence shell of the considered species. Evaluation of LI will give information of how likely is it to find

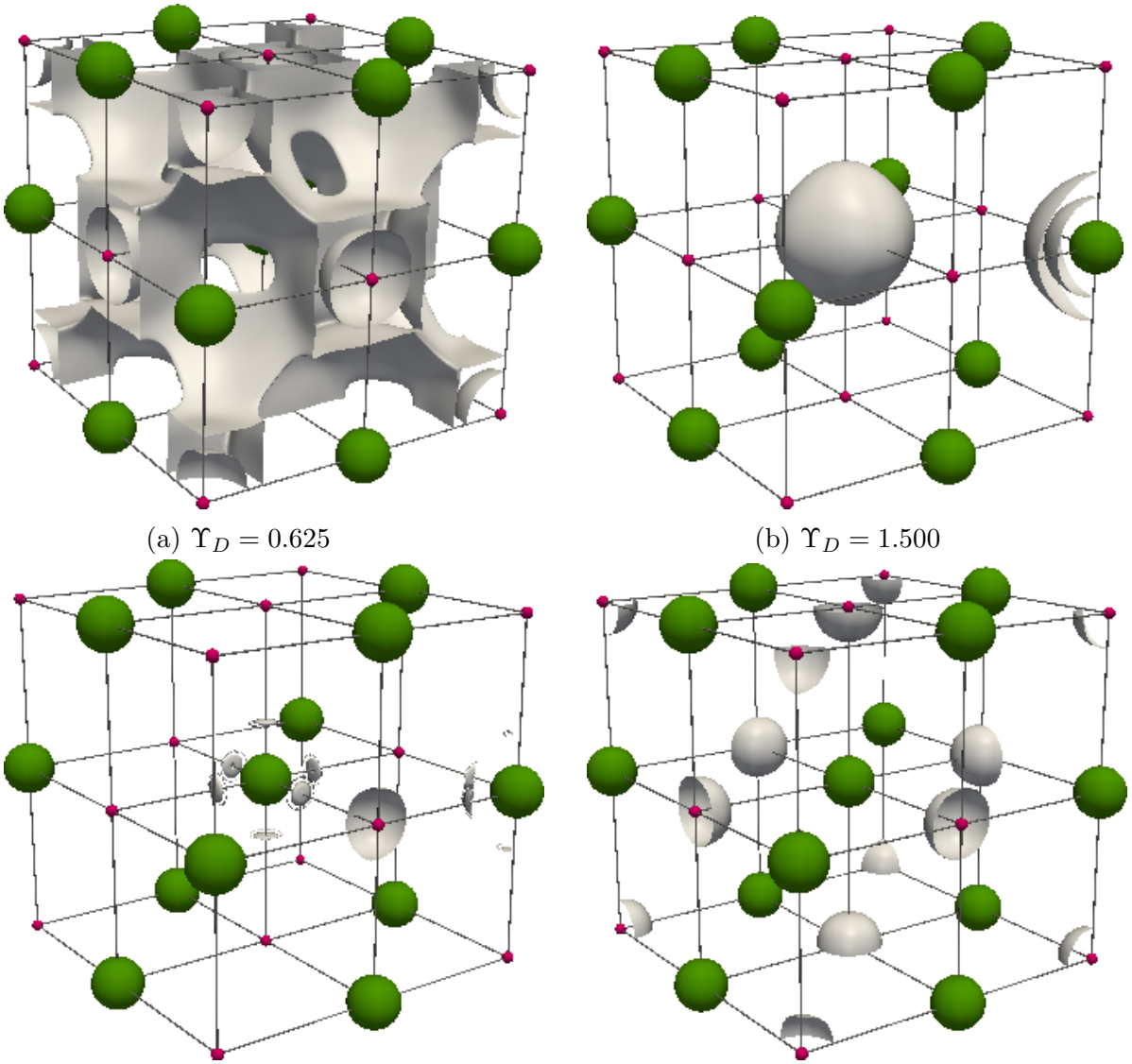

(a) $\Upsilon_D = 0.625$ (b) $\Upsilon_D = 1.500$

(c) $\Upsilon_D = 1.590$ (d) $\Upsilon_D = 1.600$

Figure 2.4.: ELI-D isosurfaces LiCl for four different Υ_D values. The reducible domain in (a) includes a few attractors; this number is reduced when increasin the isovalue (b) and becomes irreducible in (c). If the isovalue is further increased the topological type is not alter but ruther disappears.

an electron within this basin; and DI between two basins will yield information of the sharing of electrons between core-core, core-bonding or bonding-bonding basins.

2.4. Localization and Delocalization indices

In the fundamental book of QTAIM theory written by professor R.F.W. Bader in the early 1960s [3] it is given the description of certain indices, namely LI and DI, that allow us to determine the extent to which some average number of electrons are linked to a portion of the total space available to them. For a more detailed description of LI and DI the reader is referred to the references [6], [34], [35], [36] and [37]. The information about the localization of electronic charge is carried by the quantum mechanical distribution function $\Psi^*\Psi d\boldsymbol{x}_1 d\boldsymbol{x}_2 \dots d\boldsymbol{x}_N$ (see Eq. 2.36). For a system of N electrons divided into Ω regions

$$P_n(\Omega) = \frac{N!}{n!(N-n)!} \int_\Omega d\boldsymbol{x}_1 \cdots \int_\Omega d\boldsymbol{x}_n \int_{\Omega'} d\boldsymbol{x}_{n+1} \cdots \int_{\Omega'} d\boldsymbol{x}_N \Gamma^{(N)}(\boldsymbol{x}_1, \boldsymbol{x}_2, \dots \boldsymbol{x}_N), \tag{2.74}$$

$P_n(\Omega)$ is the event probability that n electrons occupy Ω while the other are in Ω'. $\Gamma^{(N)}$ is the diagonal part of the spinless N-particle density matrix as described in Eq. 2.36 —summing up spins—. $\boldsymbol{x}_i$ keeps its usual meaning. Since the wave function is normalized the summation over all possible events

$$\sum_n P_n(\Omega) = 1. \tag{2.75}$$

Integration of Eq. 2.38 over the region Ω yields the average number of particles within that region

$$\bar{N}(\Omega) = \sum_n n P_n(\Omega) = \int_\Omega \rho(\boldsymbol{r}) d\boldsymbol{r}. \tag{2.76}$$

For the electrons of a system to be fully localized one of the events described in Eq. 2.74 has to have a probability close to one whereas the remaining are zero. In other words, it is very relevant to have a expression that carries the information of to what extent the expression 2.75 is determined by just one probability whilst the rest are negligible and can be dropped out, i.e., a single event dominates the distribution. The fluctuation function closely describes this information and does not require the evaluation of the full Nth-order density matrix $\Gamma^{(N)}$. It is rather fully expressed in terms of the diagonal elements of the second-order density matrix described in Eq. 2.40.

The fluctuation in the average number of electrons in a region Ω is evaluated as

$$\sigma^2(\Omega) = \bar{N^2}(\Omega) - (\bar{N}(\Omega))^2 = \sum_n n^2 P_n(\Omega) - \Big(\sum_n n P_n(\Omega) \Big)^2, \tag{2.77}$$

which could also be expressed in terms of the second-order density matrix. That

possibility entails a *"great conceptual advantage since the extent to which a set of indistinguishable particles is spatially localized is determined by the system's pair density"*, literally quoting R.F.W. Bader [3], the distribution that also determines the fluctuation σ^2. The relevant properties of the pair density function for a system of electrons are a consequence of the Fermi correlation, which results from the antisymmetrization of the wave function required by the Pauli principle. The correlation causes the pair density function to deviate from a simple product of independent densities. This correlation is carried by the function $f(\boldsymbol{r}_1, \boldsymbol{r}_2)$ and the pair density is expressed as in Eq. 2.47. This correlation term measures not only the Fermi correlation —which exists among electrons with identical spins— but also the Coulomb correlation —affecting opposite spin electrons— (for a more detailed description of the Fermi and Coulomb correlation see section 2.62). According to the Pauli exclusion principle the exchange of the coordinates of two electrons of identical spin —recall that Fermi correlation occurs between same-spin electrons— causes the sign of the pair density to change (see Eq. 2.46).

The aim of the present section is to show the expression which describes *"the spatial extent of the effects of the self-pairing correlation on the motion of electrons, as well as whether or not the net effect of this correlation for any one particle, the correlation hole, may be localized to one particular region of space"* [3]. In that sense the Fermi correlation is of capital relevance since it solely determines the extent to which sets of electrons may be localized in some region of real space. The pair density includes a term describing the Fermi correlation and hence the mentioned two-particle property will be of great importance.

The average number of pairs of σ-spin electrons in a region can be expressed in terms of event probabilities

$$D_2(\Omega,\Omega) = \frac{1}{2}\sum_{n}^{N} P_n(\Omega)(n-1)n = \frac{1}{2}(\bar{N}^2(\Omega) - \bar{N}(\Omega)). \tag{2.78}$$

This average number of electron pairs can also be expressed by integrating both coordinates of the pair density 2.47 over the region Ω yielding

$$D_2(\Omega,\Omega) = \int_\Omega d\boldsymbol{r}_1 \int_\Omega \rho(\boldsymbol{r}_1,\boldsymbol{r}_2) d\boldsymbol{r}_2 = \frac{1}{2}\big[\bar{N}^2(\Omega) + F(\Omega,\Omega)\big], \tag{2.79}$$

$F(\Omega,\Omega)$ accounts for the correlation of the σ-spin electrons

$$F(\Omega,\Omega) = \int_\Omega d\boldsymbol{r}_1 \int_\Omega \rho(\boldsymbol{r}_1)\rho(\boldsymbol{r}_2) f(\boldsymbol{r}_1,\boldsymbol{r}_2) d\boldsymbol{r}_2. \tag{2.80}$$

A limiting situation will occur when the probability of one particular event $P_n(\Omega)$ equals unity whilst the other probabilities of the remaining events vanish. In such situation the summatory in Eq. 2.78 reduces to just one term and the pair population within the region will be $n(n-1)/2$ and it is referred to as a "pure pair" population. Electrons are uncorrelated and hence perfectly localized within

the region Ω. They behave as distinguishable particles that do not see each other and the wave function for the total system could be written as a simple product of separately antisymmetrized wave functions, with n electrons in Ω and the remaining $N-n$ in Ω'. The magnitude $F(\Omega)$ is a measure of the total Fermi hole of the $N(\Omega)$ particles that lies within the region Ω. In such limiting situation the Fermi hole for any of the n electrons in Ω is entirely contained in this region.

The term $F(\Omega,\Omega)$ is normally far from this ideal situation and normally the Fermi hole of the electrons in Ω extends out of region Ω. The magnitude $F(\Omega,\Omega)$ is given the name atomic *localization index* $\lambda(\Omega)$ [38].

It can be also measured how much of the Fermi hole of the electrons occupying a region A is localized not in the same but within a different region B. This information is contained in $F(A,B)$ which is defined in the expression for the average number of pairs of electrons formed between the electrons located at A and the electrons located at B. It is obtained by integrating the coordinates of one electron over region A and the coordinates of the other over region B

$$D_2(A,B) = \int_A d\boldsymbol{r}_1 \int_B \rho(\boldsymbol{r}_1,\boldsymbol{r}_2) d\boldsymbol{r}_2 = \frac{1}{2}\big[\bar{N}(A)\bar{N}(B) + F(A,B)\big], \tag{2.81}$$

where $F(A,B) = F(B,A)$. The sum of both magnitudes $F(A,B) + F(B,A)$ defines the delocalization index $\delta(A,B)$ and quantitatively measures the sharing of electrons between regions A and B [38].

The number of electrons $N(A)$ —charge— in the region A can be expressed as

$$N(A) = \lambda(A) + \frac{1}{2}\sum_{X\neq A}\delta(A,X), \tag{2.82}$$

and the fluctuation $\sigma^2(A)$ may be written as

$$\sigma^2(A) = D_2(A) + N(A) - N^2(A) \tag{2.83}$$

$$= N(A) - \lambda(A) = \frac{1}{2}\sum\sum_{X\neq A}\delta(A,X), \tag{2.84}$$

from where it can be seen that the variance is given by the electron and electron pair populations. For situations where the electrons are perfectly localized, that is $\lambda(A) = N(A)$, the fluctuation $\sigma^2(A)$ will attain a value of zero.

The fluctuation defined in 2.83 measures the varianze between the number of electrons occupying a region of the space and the localization of electrons within this region. Unlike in an isolated molecule, electrons a region of the space within a solid can be shared between *close* or *distant* regions. We name close regions

those having common zero-flux surfaces, that is, having direct contact with the region occupied by the electrons, whereas distant refers to regions located beyond the first neighbourhood. As defined in [39] the number of close shared pairs $\varsigma_c(A)$ for basin A is the sum of the DI of the nearest basins

$$\varsigma_c(A) = \sum_{B \neq A} \delta(A, B). \tag{2.85}$$

The difference between twice the fluctuation (total shared pairs) and the sharing among the closest basins $\varsigma_c(A)$ yields the distant shared pairs $\varsigma_d(A)$ for basin A

$$\varsigma_d(A) = 2\sigma^2(A) - \varsigma_c(A). \tag{2.86}$$

Finally, it will be meaningful to express the fraction of the total shared electron pairs that are shared with distant basins $\varkappa(A)$

$$\varkappa(A) = \frac{\varsigma_d(A)}{\sigma^2(A)}. \tag{2.87}$$

2.4.1. Delocalization indices from solid state APW DFT calculations

The calculation of DI between region A and B, denoted by $\delta(A, B)$, the part of the pair density carrying the exchange-correlation information has to be integrated as becomes clear from Eq. 2.80. The exchange-correlation part of the pair density is not explicitly available from DFT and a workaround has to be applied to build it from the Kohn-Sham orbitals using a HF-like formula (see [39] and references therein). This approach is known to yield good results in molecules and it may be also used in solid-state DFT, although partially occupied KS orbitals may appear (mostly in metals, where there are partially occupied bands).

In solid state calculations the integration to find the DI is done over the Brillouin Zone (BZ) of volume V_{BZ} which is transformed into a summation over a user-chosen number of $\vec{k}$-points within BZ (K_{BZ})

$$\delta(A, B) = \frac{2}{K_{BZ}^2} \sum_{n,n'} \sum_{\vec{k},\vec{k}'} S_{n\vec{k},n'\vec{k}'}(A) S_{n'\vec{k}',n\vec{k}}(B) \theta(n, \vec{k}) \theta(n'\vec{k}'), \tag{2.88}$$

which is the Ángyán form of the DI [40]. Also an alternative form of LI and DI as defined by Ponec can be found in [41]. The index n runs over the bands and the occupation number $\theta(n, \vec{k})$ select only occupied states. S are the overlap integrals between the KS orbitals of the crystal calculated over the region Ω

$$S_{n\vec{k},n'\vec{k}'}(\Omega) = \int_{\Omega} \psi^*_{n,\vec{k}}(\boldsymbol{r}) \psi_{n',\vec{k}'}(\boldsymbol{r}) d\boldsymbol{r}. \tag{2.89}$$

In a equivalent manner the LI over the region A are calculated as

$$\lambda(A) = \sum_{n,n'} \sum_{\vec{k},\vec{k}'} S^2_{n\vec{k},n'\vec{k}'}(A). \tag{2.90}$$

2.4.2. QTAIM Vs. ELI-D space partitioning

It was previously explained what QTAIM (section 2.3) and ELI-D basins (section 2.3.2) consist of. To summarize, QTAIM space partitioning consiststs of a coarse-grained analysis of the chemical bonding situation with each basin corresponding to one atom. On the contrary, ELI-D decomposes the space into regions corresponding to core, bonding or non-bonding localization domains. The bonding situation can be analyzed by inspection of LI and DI over QTAIM basins and more in detail over ELI-D basins.

3. Computational methods

Elk [16] is an all-electron full-potential linearised augmented-plane wave (FP-LAPW) code, one of the most accurate computational schemes for solid-state DFT [42], originally written at Karl-Franzens-Universität Graz as a milestone of the EXCITING EU Research and Training Network. In our calculations, the first step consists of a single point calculation with this code and as so we believe necessary a brief explanation of the basic theoretical concepts it is built upon.

3.1. The family of (L)APW methods

The Kohn-Sham equations are solved using a basis set that approximates the wavefunction of the solid state hamiltonian. Ideally this basis set satisfies two requirements: it should be *unbiased*: approximate wavefunctions carry too much information from the basis functions and errors are introduced to the system wavefunction; and *efficient*, only a few basis functions are necessary if they are similar to the wavefunction which is to be expanded. In summary, we are seeking a basis set efficient and simple; both requirements are satisfied by plane-waves in real space:

$$f(\vec{r}) = e^{i\vec{g}\cdot\vec{r}} \quad , \tag{3.1}$$

where $\vec{g}$ is any vector in *reciprocal space* also known as *momentum space*, which is the wave number with dimensions [1/length]. Any vector in the reciprocal space can be expressed as $\vec{g} = \vec{k} + \vec{G}$: a sum of a vector in the first Brillouin zone $\vec{k}$ plus a reciprocal lattice vector $\vec{G}$.

Block's theorem states that any eigenfunction $\psi^n_{\vec{k}}$ of a periodic hamiltonian can be expanded using a basis set of the form:

$$\psi^n_{\vec{k}}(\vec{r}) = \sum_{\vec{G}} c^{n,\vec{k}}_{\vec{G}} e^{i(\vec{k}+\vec{G})\cdot\vec{r}} \quad . \tag{3.2}$$

The part to be determined are the coefficients $c^{n,\vec{k}}_{\vec{G}}$. It can be seen from the previous expression that the wavefunction is both dependent on the Brillouin zone designated by n (also called the *band index*) and $\vec{k}$. For a certain $\vec{k}$ value within a determined Brillouin zone n, the wavefunction is hence expanded as a sum over the discrete though infinite basis set determined by $\vec{G}$. However, in practice the

infinite sum is truncated limiting the set of all $\vec{G}$ to $G \leq G_{max}$. This limits the choice of $\vec{G}$ to only the vectors contained within a sphere with radius G_{max}. This "cut-off" value, also known as *energy cut-off* or *plane-wave cut-off* is of great importance in solid state calculations since it controls the number of plane-waves that are to be used by the code.

The usage of plane-waves to approximate the wavefunction of spatially periodic hamiltonians, namely hamiltonians for crystal systems, was first introduced by Slater in 1937[43]. It is certainly advantageous to use such a expansion due to the aforementioned simplicity and moderate computational cost of the plane- wave treatment. Nevertheless a serious problem arises when trying to properly describe the region close to the nucleus.

The greater oscillation of the wavefunction affect the tails that stretch into regions close to the nucleus. However this region of the solid is quite shielded from the outer chemically relevant levels. The electrons occupying these low-lying regions of a solid behave not different from free atom electrons. The potential they suffer can therefore be replaced by a smoother *pseudopotential* that yields very smooth tails of the wavefunctions close to the nucleus, requiring only a few plane- waves to describe it.

3.1.1. The APW method

The pseudopotential method is very useful in many situations but:

- the choice of a pseudopotential is to a certain extent arbitrary
- information contained in regions close to the nucleus is lost

The first improvement of the quality of the basis set is achieved by the *Augmented Plane-Wave* basis set. The APW method is motivated by the different behaviour of electrons close and far from the nucleus, as was the pseudopotential approximation. Space is partitioned into the "muffin tin" and the "interstitial" regions. The muffin tin region is delimited by a sphere with radius R_α around each atom where electrons behave similar to free atom electrons: the muffin tin sphere comprises the region where a pseudopotential was used. The interstitial region is the space between muffin tin regions where electrons, far from the nucleus, behave as free electrons. Plane- waves are appropriate to treat free electrons (interstitial region) while atomic-like functions are suitable to describe the low-lying electrons (muffin tin region).

$$\phi_{\vec{G}}^{APW}(\vec{r}, E) = \begin{cases} \dfrac{1}{\sqrt{V}}\, e^{i(\vec{k}+\vec{G})\cdot\vec{r}} & r \in I \\ \displaystyle\sum_{l,m} a_{l,m}^{\alpha,(\vec{k}+\vec{G})}\, u_l^\alpha(r', E)\, Y_{l,m}(\hat{r}') & r' < R_{MT}^\alpha \end{cases} \tag{3.3}$$

The APW basis functions consist of plane-waves in the interstitial region that are augmented inside the MT spheres into radial solutions of the Schrödinger equation.

The symbols $\vec{k}$, $\vec{G}$ and $\vec{r}$ maintain their usual meaning and V is the volume of the unit cell in the real space. The coefficient $a_{l,m}^{\alpha,(\vec{k}+\vec{G})}$ and E are still undetermined and u_l^α are radial functions that are numerical solutions to the Schrödinger equation. Every radial function corresponds to a solution for the electron α with energy E.

The determination of the parameter $a_{l,m}^{\alpha,(\vec{k}+\vec{G})}$ is done by imposing the plane-wave to match the function inside the MT over the whole sphere surface. Each plane-wave is then expanded at $r = r_{MT}$ into spherical harmonics, which yields an infinite number of coefficients that have to be truncated at some value l_{max} [1].

However APW method is not of practical use any more today due to its energy dependence. In order to describe an eigenstate $\psi_{\vec{k}}^n(\vec{r})$ properly the energy E for that state has to be set equal to the eigenvalue (or band energy) $\epsilon_{\vec{k}}^n$ of that state. But this eigenvalue is exactly what we are looking for. The search must hence start from an initial guess of $\epsilon_{\vec{k}}^n$ for which the APW functions are evaluated, and whose result feeds the E of the next iteration and so on. The method becomes thus too slow to be applied to real systems and further improvements must be achived.

3.1.2. Linearized Augmented Plane-Wave method

The LAPW method was firstly developed by [44, 45]. A two-term Taylor expansion of the radial function $u_l^\alpha(r', \epsilon_{\vec{k}}^n)$ introduces a new term to the APW radial function that corrects it together with a new coefficient. The radial function is then expanded into a linear combination of the radial function evaluated at some fixed linearization energy E_0 and the new term: its energy derivative computed at the same energy.

$$u_l^\alpha(r', \epsilon_{\vec{k}}^n) = u_l^\alpha(r', E_0) + (E_0 - \epsilon_{\vec{k}}^n) \underbrace{\left.\frac{\partial u_l^\alpha(r', E)}{\partial E}\right|_{E=E_0}}_{\dot{u}_l^\alpha(r', E_0)} . \tag{3.4}$$

The energy difference is yet unknown and as a consequence the new coefficient $b_{lm}^{\alpha,\vec{k}+\vec{G}}$ appears.

[1] The boundary condition that both functions have to match at the sphere boundary requires the number of nodes per unit length of the plane-waves (G_{max}) to be similar to that of the angular functions (l_{max}): $R_\alpha G_{max} = l_{max}$ [23].

$$\phi_{\vec{G}}^{LAPW}(\vec{r}) = \begin{cases} \dfrac{1}{\sqrt{V}}\, e^{i(\vec{k}+\vec{G})\cdot\vec{r}} & r \in I \\ \displaystyle\sum_{l,m} \left(a_{l,m}^{\alpha,(\vec{k}+\vec{G})}\, u_l^{\alpha}(r', E_{1,l}^{\alpha}) \;+\; b_{l,m}^{\alpha,(\vec{k}+\vec{G})}\, \dot{u}_l^{\alpha}(r', E_{1,l}^{\alpha}) \right) Y_{l,m}(\hat{r}') & r' < R_{MT}^{\alpha} \end{cases} \tag{3.5}$$

The relative weight of u and $\dot{u}$ does the matching between the radial function and the plane-wave both in value and slope at the MT radius, i.e. the coefficients $b_{lm}^{\alpha,\vec{k}+\vec{G}}$ and $a_{lm}^{\alpha,\vec{k}+\vec{G}}$. The LAPWs provide the basis flexibility necessary to properly describe eigenfunctions with eigenenergies close to the linearization energy, which is kept fixed.

The energy E_0 is not universally chosen. A different energy is rather used for every angular momentum l, confering s-, p-, d- or f- character to the basis set hence adequately describing the state. Consequently E_0 is replaced by a set of well-chosen $E_{1,l}^{\alpha}$ up to $l = 3$. For higher l a fixed energy value can be used. The same procedure can now be used as for the APW method, but the secular equation that must be solved becomes linear in energy and all eigenvalues can be obtained with a single diagonalization of the secular matrix in contrast to APW.

3.1.3. LAPW with Local Orbitals: LAPW + LO

The LAPW method, though being among the most accurate applicable techniques for density-functional-based electronic-structure and total-energy calculations, has some shortcomings, the most important one arising from the linearization. The electrons lying close to the nucleus are called “core states” and behave quite like free atom electrons. They do not have an important role in chemical bonding and must lay completely inside the MT sphere. However states situated far from the nucleus leak out of the muffin tin spheres sticking into the interstitial region. Such states are named “valence states” and participate on the chemical bonding. As a third group, electrons with the same l but different principal quantum number than valence electrons, *low-lying valence states*, located in between core and valence states may have an important role in the chemical bond. For atoms with such states, called “semicore states”, the basis functions are only approximately orthogonal to the semicore states. The energies may then have a dependency on the linearization energy that has been chosen. LAPW basis is a good basis set only for eigenvalues close to the linearization energy E_l. Valence electrons sharing l with semicore states are poorly described since the E_l chosen is close to the eigenvalue of the semicore bands. As E_l is arised towards the valence bands semicore state will become poorer described and its eigenvalue will increase. At some point it will overlap with valence eigenenergies and a ghost

state will appear, preventing the total energy to be calculated.

Singh *et al.*[46] proposed a method to solve these dificulties by a change in the linearization that incorporates sufficient variational freedom to properly treat both semicore and valence states. All l except those for which there are semicore states are treated exactly as by the LAPW method, with one $u_l(r)$ and one $\dot{u}_l(r)$. Those l for which there are semicore states are described by the usual $u_l(r)$ and $\dot{u}_l(r)$ at the linearization energy $E_{1,l}$ in the valence region, supplemented by a second $u_l(r)$ for the l of the semicore states, at a second linearization energy $E_{2,l}$. A new type of basis function is added to the standard LAPW basis set, named *local orbital* (LO).

$$\phi_{l,m}^{\alpha,LO}(\vec{r}) = \begin{cases} 0 & r \in I \\ \left[a_{l,m}^{\alpha,LO}\, u_l^{\alpha}(r', E_{1,l}^{\alpha}) \;+\; b_{l,m}^{\alpha,LO}\, \dot{u}_l^{\alpha}(r', E_{1,l}^{\alpha}) \;+\; c_{l,m}^{\alpha,LO}\, u_l^{\alpha}(r', E_{2,l}^{\alpha})\right] Y_{l,m}(\hat{r}') & r' < R_{MT}^{\alpha} \end{cases} \tag{3.6}$$

This new type of basis function is only applied for certain l, for which there are semicore states and is called *local* since it does not match the plane-waves in the interstitial region. A new boundary condition is added: the basis function must be continous in value and slope at the MT radius and additionally, goes to zero at the sphere boundary $r \geq R_{MT}$. These boundary conditions allow to find the coefficients $a_{l,m}^{\alpha,LO}$, $b_{l,m}^{\alpha,LO}$ and $c_{l,m}^{\alpha,LO}$.

3.1.4. The APW-lo method

The linearization of the pure APW basis functions made in the LAPW method is energy-dependent. This was removed at the cost of a somewhat larger basis set size in the LAPW + LO method. Sjöstedt *et al.* [47] proposed a new method that expands the wave function by means of a energy-independent basis set that still has the same size as the APW basis set.

The APW + lo method provides higher variational freedom using a complementary basis set consisting of local orbitals for physically important l-quantum numbers, generally $l \leq 3$.

The orbitals used in the APW + lo are local in the same sense as used by Singh [46] to treat semicore states: they are totally confined inside the MF spheres.

Therefore the APW + lo method consists of two different kinds of basis functions: APWs and los. The first kind are exactly the same as described in 3.1.1 eq. (3.3). The second are of the form:

$$\phi_{l,m}^{\alpha,lo}(\vec{r}) = \begin{cases} 0 & r \in I \\ \sum_{l,m} \left(a_{l,m}^{\alpha,lo}\, u_l^{\alpha}(r', E_{1,l}) \;+\; b_{l,m}^{\alpha,lo}\, \dot{u}_l^{\alpha}(r', E_{1,l}) \right) Y_{l,m}(\hat{r}') & r' < R_{MT}^{\alpha} \end{cases} \tag{3.7}$$

The energies $E_{1,l}^{\alpha}$ used is the same as for the corresponding APWs. The two coefficients are found by requering the functions to be normalized $a_{lm}^{\alpha,lo}$ and that they vanish at the MT sphere boundary $b_{lm}^{\alpha,lo}$. Energies are found as in the LAPW + LO method by a single matrix diagonalization but requiring a lower plane-wave cut-off and hence similar number as APW but less functions than LAPW + LO.

APW + lo basis set appears not only to be faster than LAPW but also to provide a better description of eigenfunctions close to $E_{1,l}^{\alpha}$. Both $u_l(r, E_{1,l}^{\alpha})$ as used by APW for efficient description of eigenfunctions close to $E_{1,l}^{\alpha}$, and a more relaxed linear combination of $u_l(r, E_{1,l}^{\alpha})$ and $\dot{u}_l(r, E_{1,l}^{\alpha})$ to make an accurate description of states away from $E_{1,l}^{\alpha}$, are included in the APW + lo method.

3.1.5. Mixed basis sets

A combination of some of these methods may be suitable to treat certain special systems in which situations better treated by some of the described methods come together.

LAPW with APW + lo basis sets can solve situations hardly handled by LAPW as atoms with d- and f- valence states or systems whose atoms have very different muffin tin spheres. APW + lo basis set is used only where it is needed while the rest of the electrons are treated with LAPW.

APW + lo with LO. The same problem with semicore states that APW method had, solved with LAPW + LO in section 3.1.3 is encoutered in the APW + lo. LOs used for APW + lo look however differently:

$$\phi_{l,m}^{\alpha,LO}(\vec{r}) = \begin{cases} 0 & r \in I \\ \left[a_{l,m}^{\alpha,LO}\, u_l^{\alpha}(r', E_{1,l}^{\alpha}) \;+\; c_{l,m}^{\alpha,LO}\, u_l^{\alpha}(r', E_{2,l}^{\alpha}) \right] Y_{l,m}(\hat{r}') & r' < R_{MT}^{\alpha} \end{cases} \tag{3.8}$$

3.2. Computational details

Convergence tests for all systems evaluated in this work have been performed against the number of k-points and the parameter `rgkmax`.

The number of k-points is controlled by the parameter `ngridk`. The integrations necessary to perform a ground state (GS) calculation are done over the first Brillouin Zone (BZ). However, this volume has to be discretized and the the integrals become sums evaluated at certain points of a 3D grid on the BZ. The size of this grid is determined by the number of k-points into which the grid is divided in each direction. In that way a calculation using Elk with `ngridk` $= 8$ will have to evaluate 8^3 sums, 8 on each direction of real space. As it controls the number of integral evaluations that must be performed directly determines the computational cost of the calculation. But too coarse-grained grids lead to very unaccurate results from which no useful information may be obtained. That explains the importance of a convergence test to find a good comprimise between accuracy and computational cost.

Convergence test of the parameter `ngridk` for the systems under study are included in Figs. 3.2. The convergence was attained for a number of k-points $= 6$ as can be seen from Fig. 3.2. The grid size not only determined the computational cost of the GS calculation with Elk; the evaluation of the overlap integrals, task performed by DGrid is also a very time-demanding calculation that can sometimes be prohibited. Due to the time-consuming evaluation of overlap integrals —even using 8 processors in the calculation— and the large amount of memory required a number of k-points equal to 2 has been used for all systems except for *bcc* K, where 6 k-points were used (Table 3.1). More powerful computers should have been used in order to get more accurate and hence reliable results.

Once the optimal number of k-points has been determined convergence was checked against the parameter `rgkmax`. It represents the product of two quantities: R_{min}^{MT} which is the smallest muffin-tin radius of all the atoms participating in the calculation; and $|\boldsymbol{G}+\boldsymbol{k}|_{max}$, which limits the maximum length for the $\boldsymbol{G}+\boldsymbol{k}$ vectors, defined as `rgkmax` divided by the smallest muffin-tin radius (see Table 3.1. Each of these vectors stands for one basis function which means that this parameter determines the number of basis functions used to solve the Kohn-Sham equations. It is one of the crucial parameters for a solid state calculation and as so has been checked for convergence. All calculations has been done with a value of `rgkmax` equal to 9.

Another relevant parameter is `lradstp`. In order to save computational time some muffin-tin functions such as density are firstly evaluated on a coarse-grained mesh and afterwards interpolated into a finer one. This parameter determines the step size when going from the coarse to the fine mesh and hence it may be crucial for runnings where the electron density is a property of interest and properties

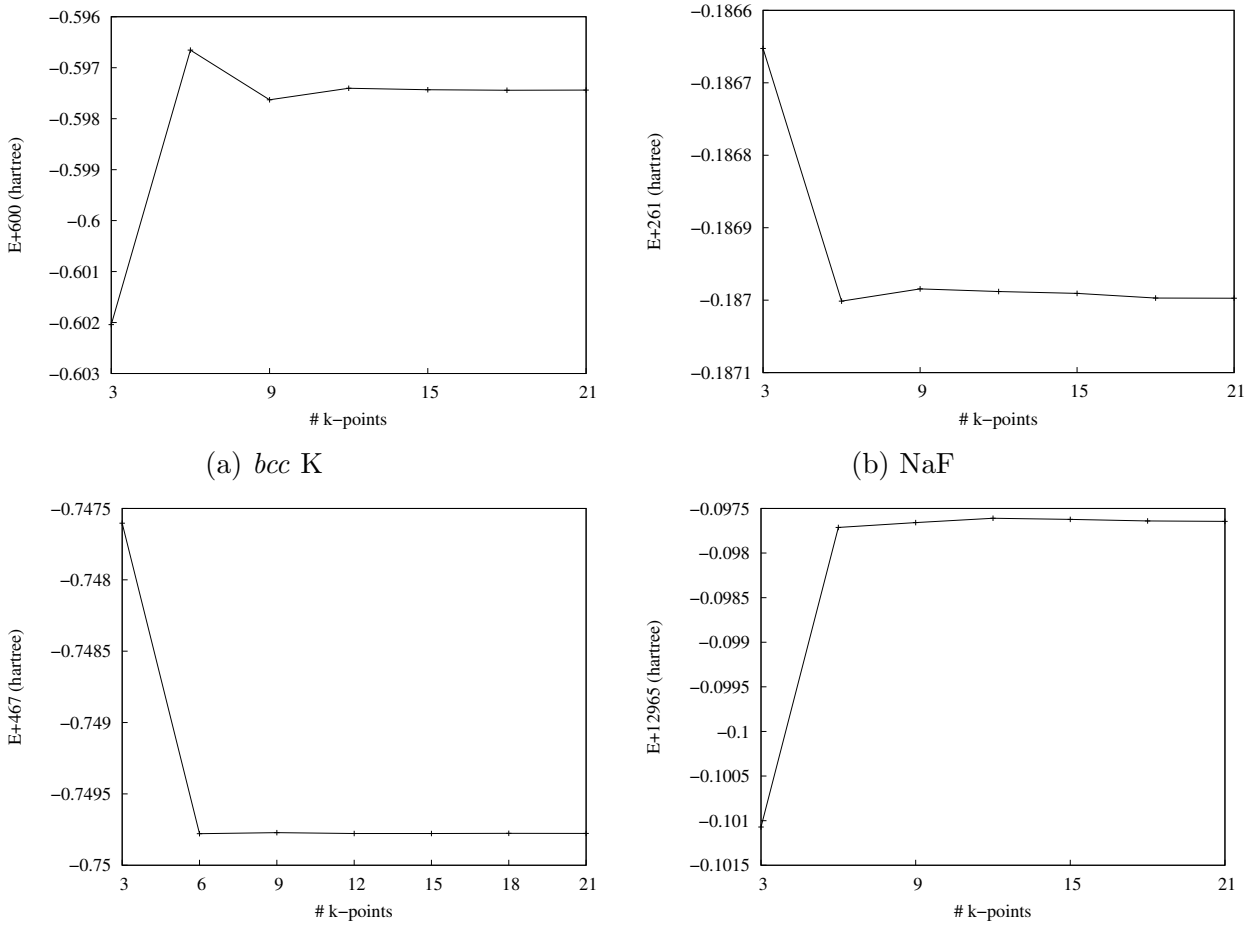

(a) *bcc* K (b) NaF

(c) LiCl (d) SnTe

Figure 3.1.: Convergence of the total energy [*hartree*] with respect to the number of k-points for the 4 crystals used.

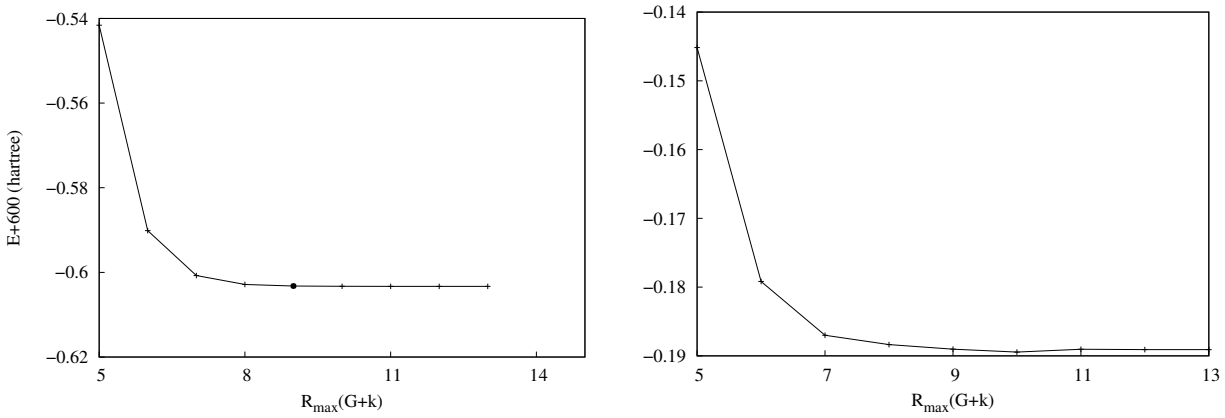

(a) *bcc* K (b) NaF

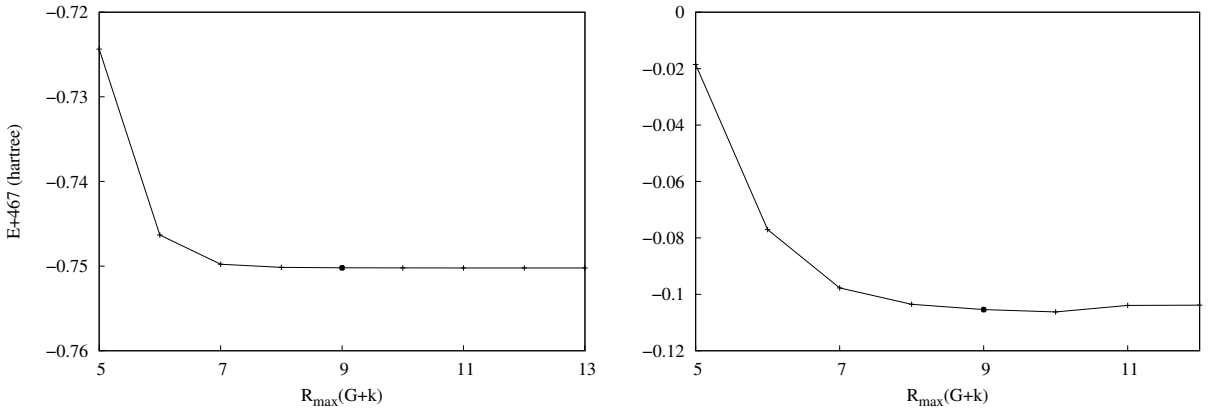

(c) LiCl (d) SnTe

Figure 3.2.: Convergence of the total energy [*hartree*] with respect to `rgkmax` (see Table 3.1 and text for details). The black point indicates the value of `rgkmax` chosen for the calculations.

Table 3.1.: Detailed values of Elk parameters used in the calculations.

System	*bcc* K	NaF	LiCl	SnTe	Meaning
Cell (a.u.)	9.9154	8.7305	9.6934	11.9300	
`ngridk`	6	2	2	2	k-point mesh size $= ngridk^3$
`rgkmax`	9	9	9	9	$R_{min}^{MT} \times \max\{\|\boldsymbol{G}+\boldsymbol{k}\|\}$
`gmaxvr`	14.0	13.0	12.0	12.0	maximum length of $\|\boldsymbol{G}\|$ for the potential and density expansion in the interstitial region

derived from it such as ELF or ELI-D. To ensure continuity at the boundary between the muffin-tin and the interstitial region a value of `lradstp` = 1 was used in all the calculations.

Parameters whose default value has been used are not included in 3.1, such as expansions of the angular momentum on both muffin-tin and interstitial region, but their effect may be relevant for certain calculations.

The next step consists in constructing a grid with values of electron density and ELI-D, grid that we will use to partition the space into basins and lately evaluate the overlap integrals. This task is performed by the code DGrid [1], a program capable of the generation of property values on an equidistant grid. The separation between consecutive grid points needs to be ideally 0.05 in order to get a fine enough mesh that allows a precise evaluation of the overlap integrals. That is defined in the first DGrid input file included for the crystal *bcc* K in the appendix (see Appendix A.1 for an example). The field resulting from this calculation can be seen with the visualization software ParaView [48] using for instance a isosurface (see Fig. 2.2).

The grid with the density and ELI-D value can be searched for basins. From electron density regions surrounded by zero-flux surfaces of the gradient are determined [3]. From ELI-D field localization domains [32], that is, regions surrounded by an isosurface, separate regions surrounded by two isosurfaces can be defined. How the QTAIM and ELI-D basins are defined can be seen in the following chapter 4. The search for basins is done with the keyword `top` (see Appendix A.3). It establishes a cut-off value for the quantity that is been treated that DGrid uses to asign all closed regions above it to the same basin. In order to chose the adequate value for the `top` keyword it is useful the visualization of the isosurfaces of the treated property. In Fig. 3.3a it can be seen a sphere surrounding the central Sn. If we have a look at a section of this sphere we see that it is formed by concentric spheres which represent the atomic shell structure of the atom.

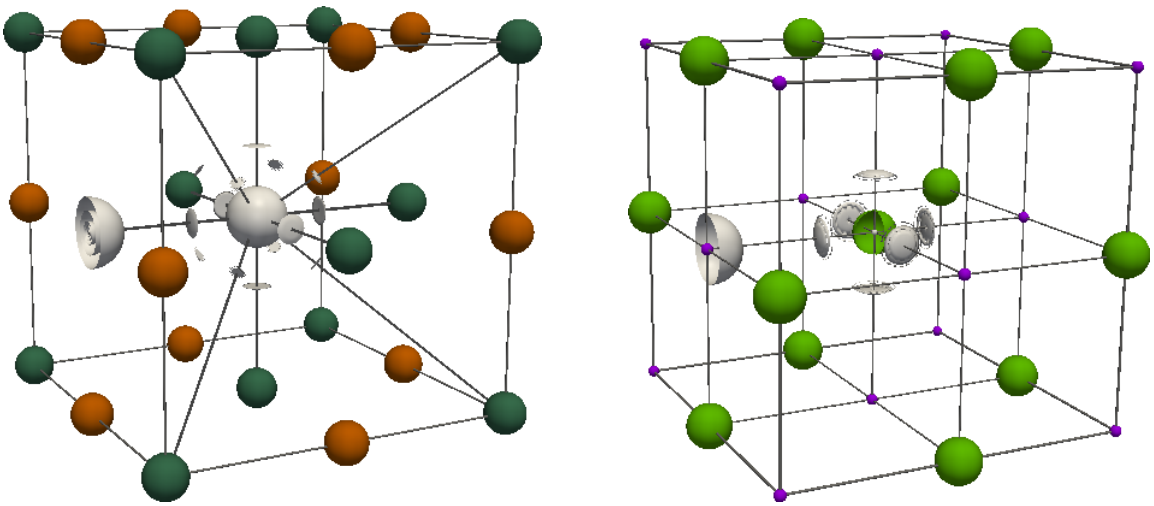

(a) SnTe (b) LiCl

Figure 3.3.: Isosurface of the ELI-D field for SnTe $\Upsilon_D = 1.23$ (left) and LiCl $\Upsilon_D = 1.585$ (right). Note the dark grey lines that go through the discs, drawn to show that each disc is centered at the connection path between two atoms.

All these spheres are automatically asigned to the same basin (with the keyword `ELI_core` (see Appendix A.3); otherwise a bunch of meaningless localization domains will be formed. For a ELI-D value of $\Upsilon_D = 1.23$ the isosurface forms some discs dispossed around the atoms [2] that are centered at the interconnection paths between the central atom and either a first (in the direction of one of the lattice vectors) or a second neighbour. The search for basins with a value `top` = 1.23 will yield a different basin for each localization domain that can be seen in 3.3a. Higher isosurface values would make the discs to fade away whilst lower values will cause them to merge together into a somewhat sphere-like surface that will yield a single basin (see 2.3.2 for a better understanding of this).

A similar situation can be seen for LiCl in Fig. 3.3b where the bonding basins 4.4 can be anticipated from the discs formed between the nearest atoms (for the sake of clarity only chosen features are shown).

If the basin search was successful the next step will consist on the evaluation of the overlap integrals over the QTAIM basins or ELI-D localization domains (see Appendix A.4). Once this overlap integrals have been evaluated LI 2.90 and DI 2.88 are calculated. It is a very demanding task regarding both the timing: 106 hours of real job time for *bcc* K for QTAIM basins and 102 for ELI-D basins; and

[2] In Fig. 3.3 the isosurface of ELI-D are shown for only certain atoms chosen on purpose to highlight the relevant features but for every atom the corresponding isosurfaces equivalent by symmetry are also present.

the memory: except for *bcc* K calculations using a number of k-points > 4 was prohibitive in nodes with 32Gb of memory.

4. Applications. Bonding descriptors in model systems

4.1. Metallic solids: bcc K

QTAIM

Table 4.1 contains the Localization (LI) and Delocalization (DI) Indices computed within the QTAIM theory for *bcc* K. Metals are believed to present high values of electron DI. According to the free electron model for the behaviour of electrons within a crystalline structure of a metallic solid, valence electrons are completely detached from their ion (like an electron gas). From Bloch's theorem and Pauli's principle unbound electrons within a periodic potential behave as free electrons in vacuum. Accordingly enhanced delocalization is expected for alcaline metals like K.

High fluctuation $\sigma^2 = 0.80$ value (Table 4.1) is observed for the K atomic core basin in comparison to that of ionic compunds ($\sigma^2(F) = 0.40$, $\sigma^2(Na) = 0.25$ in NaF). This fluctuation, defined for a basin as the difference between the population of the basin and the localization of electrons LI within it (see Eq. 2.83), is interpreted as a measure of the delocalization of the electrons over the whole solid. Each K atomic core region shares $\delta(A, B) = 0.09$ electron pairs with a neighbouring basin. Since every K basin is surrounded by 8 K basins, a total of 0.72 electron pairs are shared with the first neighbour basins. The electron pairs shared with the more distant basins, given by $\varsigma(K) = 0.88$ (see Eq. 2.86) yield a 55 % ($\varkappa = 0.55$) of the fluctuation shared with the more distant basins. A electron can delocalize to basins beyond the most inmediate basins, unlike for other non-metallic solids.

Further evaluation of the delocalization with the second neighbour basins located at 5.25 Åwould more accurately yield how far an electron can move from the K core. This has not been pursued in this work. For the also alkaline metal *bcc* Na identical fluctuations ($\sigma^2 = 0.80$) and similar DI ($\delta = 0.10$) were found for the closest basins, but a lower number of electron pairs ($\varkappa = 0.28$) are shared with the solid beyond the second neighbour basins [39].

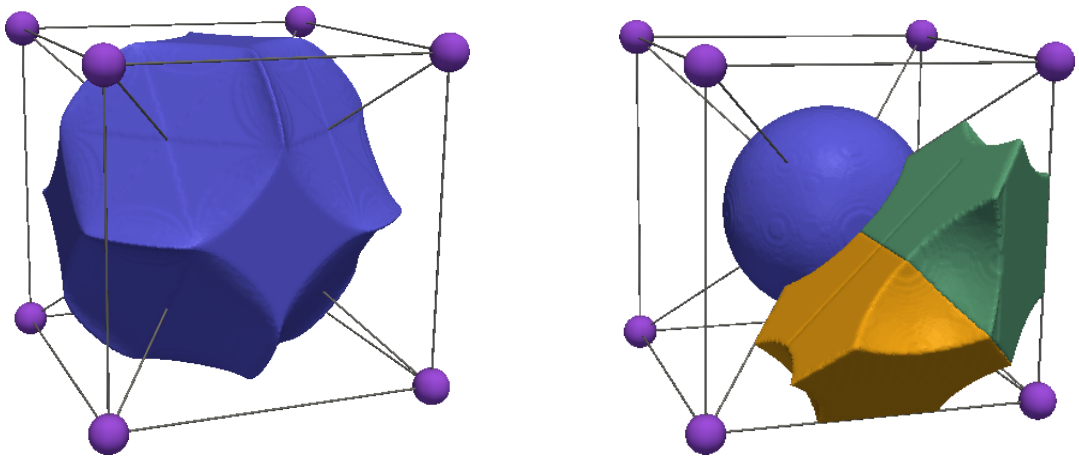

Figure 4.1.: *bcc* K basins. Left: QTAIM atomic basin of atom K (blue). Right: ELI-D core $\mathcal{C}_K$ (blue) and bonding $\mathcal{B}_{4K}$ (yellow and green) basins.

ELI-D

The atomic shell structure in real space of a free atom can be figured out by means of ELI-D. The atomic structure is seen as sphere-like basins centered at the nucleus (see Fig. 3.3) that are grouped into basins sets and further merged into superbasins in order to simply their interpretation. Such superbasins are separed into two different kinds: *atomic cores* and *bonding regions*, whose appearance is as shown Fig. 4.1 (right). Unlike the QTAIM basins which are found from the density (one-particle quantity) ELI-D basins are based on a two-particle quantity as it is the ELI-D indicator 2.73.

All LI as well as fluctuations and electron populations for ELI-D values are included in Table 4.2 whereas DI are shown in Table 4.3. As mentioned before high DI are expected for alkali metals as *bcc* K. Each bonding basin $\mathcal{B}_{4\mathrm{K}}$ — where the subindex "4K" indicates that every bonding basin is surrounded by 4 K atomic cores— has a very small population 0.15 and very high fluctuation $\sigma^2 = 0.14$ (Table 4.2). Each bonding region $\mathcal{B}_{4\mathrm{K}}$ shares 0.015 electron pairs with the K core $\mathcal{C}_{\mathrm{K}}$ (Table 4.3, Fig. 4.1) which makes a total of 0.06 electron pairs. It is also surrounded by 4 bonding basins that it shares 0.011 electron pairs with, making a total of 0.044 pairs. In total every bonding basin shares $\varsigma = 0.18$ (see Eq. 2.86) electron pairs with the rest of the solid beyond the first neighbours, that is a 64 % of the shared pairs (Table 4.3).

Each core basin $\mathcal{C}_{\mathrm{K}}$ has a very low DI $\delta = 0.004$ with each of the 8 surrounding core basins (compared with the DI with a bonding basin Table 4.3). This value ($0.004 \times 8 = 0.03$) plus the DI with the 24 bonding basins $\mathcal{B}_{4\mathrm{K}}$ ($0.015 \times 24 = 0.36$) gives a total of 0.39 electron pairs shared with the nearest neighbours, i.e., $\varsigma = 0.17$ electron pairs shares every core region $\mathcal{C}_{\mathrm{K}}$ with the rest of the solid.

As is expected for a metal the delocalization of electrons with distant basins is

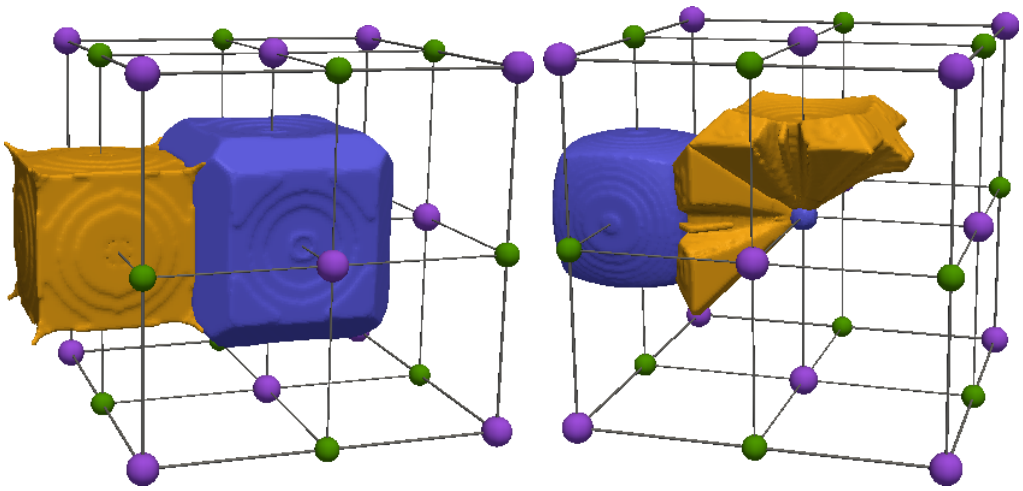

Figure 4.2.: NaF QTAIM and ELI-D basins. Left: QTAIM atomic basin for F (blue) and Na (yellow). Right: ELI-D core basins for F $\mathcal{C}_{\mathrm{F}}$ (blue, small) and Na $\mathcal{C}_{\mathrm{Na}}$ (blue, large). Bonding ELI-D basins $\mathcal{B}_{\mathrm{F(2)}}$ are shown in yellow.

higher ($\varkappa(\mathcal{B}_{\mathrm{4K}}) = 0.64$) than for crystals such as NaF ($\varkappa(\mathcal{B}_{\mathrm{NaF}}) = 0.14$) or LiCl ($\varkappa(\mathcal{B}_{\mathrm{LiCl}}) = 0.20$, Table 4.3) with ionic character.

4.2. Ionic solid: NaF and LiCl

4.2.1. NaF

QTAIM

The partition of space into atomic basins according to the QTAIM is shown in Fig. 4.2 (left). NaF is a typical ionic solid and consequently high localization of electrons $\lambda(A)$ with values close to the QTAIM basins population is expected, as long as low variances σ^2.

In Table 4.1 can be seen that LI's within Na and F basins $\lambda(\mathrm{Na}) = 10.12$ and $\lambda(\mathrm{F}) = 9.48$, respectively, are close to the respective populations $N(\mathrm{Na}) = 10.12$ and $N(\mathrm{F}) = 9.87$. Correspondingly low fluctuations (defined in Eq. 2.83) σ^2 are found in both cases, which can be compared with the *bcc* K case, with larger values as a metallic solid $\sigma^2(\mathrm{Na}) = 0.25$ and $\sigma^2(\mathrm{F}) = 0.40$ whereas $\sigma^2(\mathrm{K}) = 0.80$. Correspondingly, the distant shared electron pairs value is much higher for the metal bonding situation where the electrons are thought to be highly delocalized within the solid $\varsigma(\mathrm{K}) = 0.88$, whereas in a ionic solid the probability to find an electron far from its nucleus is very low $\varsigma(\mathrm{Na}) = 0.02$ and $\varsigma(\mathrm{F}) = 0.03$. In other words, in the ionic picture practically all the electrons ($\varkappa(\mathrm{Na}) = \varkappa(\mathrm{K}) = 0.04 = 96\%$, Table 4.1) are shared with the closest neighbours which means that the probabil-

Table 4.1.: Localization and delocalization indices for QTAIM basins.

Compound	A	$N(A)$	$\sigma^2(A)$	$\lambda(A)$	$\varsigma(A)$	$\varkappa(A)$	$A-B$	$\delta(A,B)$
bcc K	K	19.00	0.80	18.20	0.88	0.55	K-K	0.09
NaF	F	9.87	0.40	9.48	0.03	0.04	F-Na	0.08
	Na	10.12	0.25	9.87	0.02	0.04	Na-Na	0.00
							F-F	0.02
LiCl	Cl	17.89	0.63	17.26	0.06	0.05	Cl-Li	0.04
	Li	2.11	0.14	1.97	0.04	0.15	Cl-Cl	0.08
							Li-Li	0.00
SnTe	Sn	49.32	1.62	47.70	0.62	0.19	Sn-Te	0.40
	Te	52.66	1.90	50.76	0.86	0.23	Te-Te	0.07
							Sn-Sn	0.03

A: atom; N(A): atom A population within QTAIM basin; $\sigma^2(A)$: fluctuation; λ: localization index; $\varsigma(A)$: distant shared pair electrons; $\varkappa(A)$: fraction of the shared electrons delocalized whithin distant basins; $\delta(A,B)$: delocalization index between atomic basins A and B.

ity of finding an electron far from its nucleus almost vanishes when going beyond nearest basins.

It is also important to note the shape of the interatomic surfaces between the F cores. As it can be seen in Fig. 4.2 (left) the F atomic basins instead of having sharp edges and spikes as the Na basins have them cut and forming a flat plane. It is the plane of direct contact between two atomic F basins, and since Na basins do not have direct contact with each other, higher delocalization is expected to occur between F basins in contact $\delta(\mathrm{F},\mathrm{F}') = 0.02$, which is of the same order as the delocalization between Na and F basins and much higher than $\delta(\mathrm{Na},\mathrm{Na}') \approx zero$, Table 4.1.

In the classical ionic picture, anions are thought to be large, distortable and susceptible to be polarized, unlike cations which are understood to be small, rigid and not susceptible to be polarized. In that sense, when taking part in an ionic bonding situation the cations adopt convex shape occupying the pace while the anions are concave and adopt themselves to the holes the cations leave free [11].

If Fig. 4.4 (left) is observed, it can be inmediately recognized by looking at the shape of each basin which one each atom corresponds to: the yellow basin has a convex-like shape whilst the blue adapts itself to the yellow one. The yellow bsin corresponds to the cation (Li^+) and the blue one to the anion (Cl^-). In Fig. 4.2 this situation can be seen as well for the system NaF although it is not as clear as in case of the LiCl. The yellow basin (which corresponds to the cation Na^+) is convex-like whilst the blue one (corresponding to the anion F^-) adapts its shape

Table 4.2.: Localization indices in ELI-D basins.

Compound	Basin	N	σ^2	λ	ς	$\varkappa$
bcc K	$\mathcal{C}_{\mathrm{K}}$	18.10	0.28	17.82	0.17	0.30
	$\mathcal{B}_{4\mathrm{K}}$	0.15	0.14	0.01	0.18	0.64
NaF	$\mathcal{C}_{\mathrm{F}}$	2.16	0.39	1.77	0.01	0.01
	$\mathcal{C}_{\mathrm{Na}}$	10.06	0.23	9.83	0.39	0.85
	$\mathcal{B}_{\mathrm{F(2)}}$	1.28	0.81	0.47	0.23	0.14
	$\mathcal{S}[6\mathcal{B}_{\mathrm{F(2)}}]$	7.78	0.77	7.01	0.03	0.02
LiCl	$\mathcal{C}_{\mathrm{Cl}}$	10.07	0.58	9.49	0.01	0.01
	$\mathcal{C}_{\mathrm{Li}}$	2.03	0.10	1.93	0.07	0.35
	$\mathcal{B}_{\mathrm{Cl(3)}}$	1.31	0.85	0.46	0.34	0.20
	$\mathcal{S}[6\mathcal{B}_{\mathrm{Cl(3)}}]$	7.90	1.19	6.71	0.07	0.03

N: population within ELI-D basin; σ^2: fluctuation; λ: localization index; ς: distant shared electron pairs for *Basin*; $\varkappa$: fraction of the *Basin*'s shared electrons delocalized among distant basins.

to fill the space the surrounding cations leave free.

The contact between basins corresponding to the same atom must be identical and consequently the contact surface has to be flat. That is clearly observed in the case that has just been discussed, where the surface at the contact between two blue Cl^- basins is flat (Fig. 4.2), and in the LiCl for the Cl^- interatomic surfaces (Fig. 4.4). In the case of *bcc* K, since only one atom is present all the contact surfaces must be planar. However in Fig. 4.1 a somewhat concave relief can be appreciated. That is caused by the algorithm to draw the surfaces, which also provoques the concentric rings that can be seen in all the drawings (cf. for example Fig. 4.2).

ELI-D

As explained for the *bcc* K ELI-D, when applied to free atoms, reflects the atomic shell structure in real space by means of basins that can be recursively merged together to form atomic core and bonding superbasins. For ionic compounds such as NaF, the ELI-D basins show both the atomic cores, which normally present low fluctuation values σ^2 (typically between 0.1 and 0.6) and the bonding basins surrounding the anion core, that correspond to the valence electrons.

The core shell basins $\mathcal{C}_{\mathrm{F}}$ and $\mathcal{C}_{\mathrm{Na}}$ (blue basins in Fig. 4.2) are considered to be chemically inert, not contributing to bonding. They exhibit high localization and therefore low variances $\sigma^2(\mathcal{C}_{\mathrm{F}}) = 0.39$ and $\sigma^2(\mathcal{C}_{\mathrm{Na}}) = 0.23$, Table 4.2. DI values are consistently very low $\delta(\mathcal{C}_{\mathrm{Na}}, \mathcal{C}_{\mathrm{F}}) = 0.002$, Table 4.3, which is the same value found for the also ionic compound NaCl $\delta(\mathcal{C}_{\mathrm{Na}}, \mathcal{C}_{\mathrm{Cl}}) = 0.002$ in [39].

Table 4.3.: Delocalization indices between nearest ELI-D basins.

Compound	b_1	b_2	$\delta(b_1, b_2)$
bcc K	$\mathcal{C}_{\mathrm{K}}$	$\mathcal{C}_{\mathrm{K}}$	0.004
	$\mathcal{C}_{\mathrm{K}}$	$\mathcal{B}_{4\mathrm{K}}$	0.015
	$\mathcal{B}_{4\mathrm{K}}$	$\mathcal{B}_{4\mathrm{K}}$	0.011
NaF	$\mathcal{C}_{\mathrm{Na}}$	$\mathcal{C}_{\mathrm{F}}$	0.002
	$\mathcal{C}_{\mathrm{F}}$	$\mathcal{B}_{\mathrm{NaF}}$	0.126
	$\mathcal{C}_{\mathrm{Na}}$	$\mathcal{B}_{\mathrm{NaF}}$	0.009
intra	$\mathcal{B}_{\mathrm{NaF}}$	$\mathcal{B}_{\mathrm{NaF}}$	0.310
inter	$\mathcal{B}_{\mathrm{NaF}}$	$\mathcal{B}_{\mathrm{NaF}}$	0.004
LiCl	$\mathcal{C}_{\mathrm{Cl}}$	$\mathcal{C}_{\mathrm{Li}}$	0.001
	$\mathcal{C}_{\mathrm{Cl}}$	$\mathcal{B}_{\mathrm{LiCl}}$	0.191
	$\mathcal{C}_{\mathrm{Li}}$	$\mathcal{B}_{\mathrm{LiCl}}$	0.020
intra	$\mathcal{B}_{\mathrm{LiCl}}$	$\mathcal{B}_{\mathrm{LiCl}}$	0.276
inter	$\mathcal{B}_{\mathrm{LiCl}}$	$\mathcal{B}_{\mathrm{LiCl}}$	0.012

b_1: first ELI-D basin; b_2: second ELI-D basin; $\delta(b_2, b_2)$: delocalization index between both basins.

Table 4.4.: Delocalization indices between nearest ELI-D core basins and valence superbasins.

Compound	b_1	b_2	$\delta(b_1, b_2)$
NaF	$\mathcal{C}_{\mathrm{F}}$	$\mathcal{S}[6\mathcal{B}_{\mathrm{F}(2)}]$	0.756
	$\mathcal{C}_{\mathrm{Na}}$	$\mathcal{S}[6\mathcal{B}_{\mathrm{F}(2)}]$	0.072
	$\mathcal{S}[6\mathcal{B}_{\mathrm{F}(2)}]$	$\mathcal{S}[6\mathcal{B}_{\mathrm{F}(2)}]$	0.027
LiCl	$\mathcal{C}_{\mathrm{Cl}}$	$\mathcal{S}[6\mathcal{B}_{\mathrm{Cl}(3)}]$	1.135
	$\mathcal{C}_{\mathrm{Li}}$	$\mathcal{S}[6\mathcal{B}_{\mathrm{Cl}(3)}]$	0.032
	$\mathcal{S}[6\mathcal{B}_{\mathrm{Cl}(3)}]$	$\mathcal{S}[6\mathcal{B}_{\mathrm{Cl}(3)}]$	0.082

b_1: first ELI-D basin; b_2: second ELI-D basin; $\delta(b_2, b_2)$: delocalization index between both basins; $\varsigma(b_1)$: distant shared electron pairs; $\varkappa(b_1)$: fraction of the shared electrons delocalized within distant basins.

The bonding volume in NaF is formed by 6 bonding basins $\mathcal{B}_{\mathrm{F}(2)}$ (yellow volumes in Fig. 4.2) where the subscript "F(2)" indicates that the basin is associated with the 2nd shell of the F. Each separed bonding basin has high fluctuation values $\sigma^2(\mathrm{F}(2)) = 0.81$, see Table 4.2. The sharing of electrons between basins belonging to the same valence basin set, as the two yellow basins drawn in Fig. 4.2, (row "intra" in Table 4.3) is higher than that between basins of different atoms (row "inter"), close to zero: $\delta(intra) = 0.310$ and $\delta(inter) = 0.004$, respectively. Thus the 6 basins completing the valence region of F form a basin set that can be merged together into a superbasin (left, light red basin in Fig. 4.4). The shape of the superbasin formed by merging together 6 basins surrounding a F atom resembles very closely the shape of the QTAIM basin for the same atom (compare right, blue basin in Fig. 4.2 and left, light red basin in Fig. 4.4).

The LI and DI for the valence basins merged together into the superbasin $\mathcal{S}[6\mathcal{B}_{\mathrm{F}(2)}]$ are shown in Tables 4.2 and 4.4, respectively. Each superbasin shares $\delta(\mathcal{C}_{\mathrm{F}}, \mathcal{S}[6\mathcal{B}_{\mathrm{F}(2)}]) = 0.756$ electron pairs with the F atom it includes and $6 \times 0.072 = 0.432$ with the 6 $\mathcal{C}_{\mathrm{Na}}$ basins is surrounded by (cf. Table 4.3). Additionally every superbasin shares $12 \times \delta(\mathcal{S}[6\mathcal{B}_{\mathrm{F}(2)}], \mathcal{S}[6\mathcal{B}_{\mathrm{F}(2)}]) = 12 \times 0.027 = 0.324$ electron pairs with the direct neighbouring basins. That makes a total of 1.512 electron pairs shared with the closest neighbourhood and thus, only $\varsigma(\mathcal{S}[6\mathcal{B}_{\mathrm{F}(2)}]) = 2 \times 0.72 - 1.512 = 0.03$ (Table 4.2) electron pairs are shared with basins beyond the closest neighbourhood, i.e., a 2 % $\varkappa(\mathcal{S}[6\mathcal{B}_{\mathrm{F}(2)}]) = 0.02$ of the total number of shared electron pairs.

The value of the distant shared pairs for the ELI-D valence basin set $\mathcal{S}[6\mathcal{B}_{\mathrm{F}(2)}]$ is exactly the same as the one for the F atomic core found in the QTAIM analysis $\varsigma(\mathrm{F}) = 0.02$ (Table 4.1), which further supports the fusion of the 6 valence basins into one single superbasin.

Transferability assumes that a chemical property associated with an atom remains similar —though not identical— under a variety of different circumstances [49]. According to the free electron model for metallic crystals, the *bcc* K is understood to release an electron behaving as a cation K^+. When forming an ionic compound like for example KCl it behaves as a cation in the same sense as in the metal, while the Cl is the anion. Thus transferability makes us to expect the K atom to behave similarly in both situations. This has already been checked taking the fluctuation σ^2 of the Na atomic core within the ELI-D basins as the property that should be conserved, in the metallic situation *bcc* Na $\sigma^2 = 0.20$ almost identical as in the ionic compound NaCl $\sigma^2 = 0.19$ [39]. Although we have no ionic compound involving K, the Na atom in NaF is expected to closely mimic the K atom in *bcc* K. It is confirmed by analyzing the same property in both situations $\sigma^2(\mathrm{Na}) = 0.23$ in NaF and $\sigma^2(\mathrm{K}) = 0.28$ in *bcc* K where similar though somewhat different values are encountered.

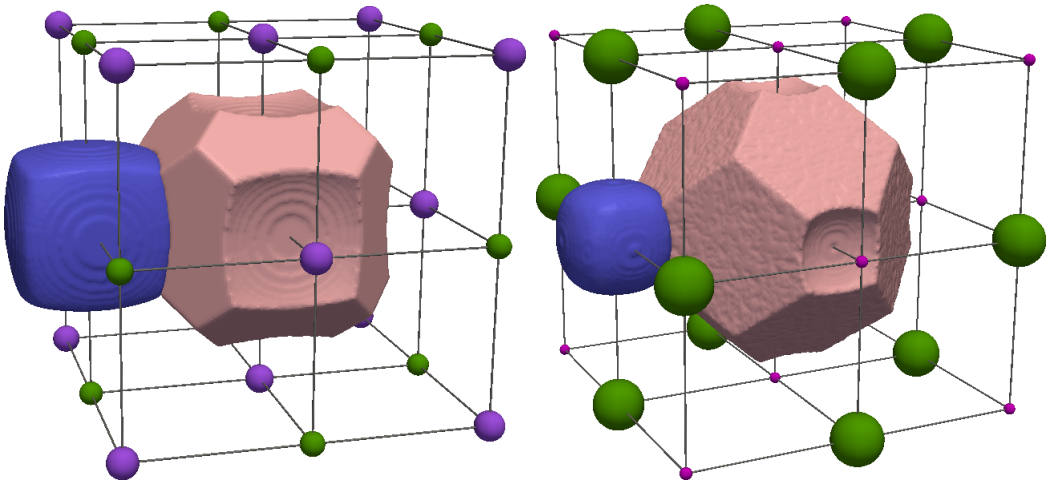

Figure 4.3.: ELI-D core basins and valence superbasins. NaF (left): Na atomic core basin $\mathcal{C}_{\mathrm{Na}}$ (blue) and F superbasin $\mathcal{S}[6\mathcal{B}_{\mathrm{F}(2)}]$ (light red). LiCl (right): Li atomic core basin $\mathcal{C}_{\mathrm{Li}}$ and Cl superbasin $\mathcal{S}[6\mathcal{B}_{\mathrm{Cl}(3)}]$ (light red).

4.2.2. LiCl

QTAIM

Being also an ionic solid, the LIs and DIs in LiCl can be compared with the results found for NaF. The localization of the electrons λ is again high with low fluctuations $\sigma^2(\mathrm{Cl}) = 0.63$ and $\sigma^2(\mathrm{Li}) = 0.14$ (see Table 4.1). The electron pairs shared with the basins beyond the first neighbourhood are very low as for NaF $\varsigma(\mathrm{Cl}) = 0.06$ and $\varsigma(\mathrm{Li}) = 0.04$ and as expected for an ionic bonding situation. The interatomic surface now between the Cl atoms where both atomic core basins touch each other gives DI values $\delta(\mathrm{Cl}-\mathrm{Cl}) = 0.08$ even higher than that between Li and Cl atoms (see Table 4.3). Note also the flat hexagon-like surfaces formed at the contact plane between two different Cl atomic core basins (Fig. 4.3).

ELI-D

The ELI-D scheme is also similar as for NaF. The localization within the ELI-D core basins are high and correspondingly the fluctuation is low $\sigma^2(\mathrm{Cl}) = 0.58$ and $\sigma^2(\mathrm{Li}) = 0.10$ (Table 4.2). The delocalization between atomic cores $\delta(\mathcal{C}_{\mathrm{Cl}}, \mathcal{C}_{\mathrm{Li}}) = 0.001$ is negligible as for the NaF case and NaCl in reference [39].

The bonding basin $\mathcal{B}_{\mathrm{Cl}(3)}$, where the subscript "Cl(3)" means asbefore that it is formed by the 3rd atomic shell of the Cl atom, shares electrons mainly with the Cl atomic core $\delta(\mathcal{C}_{\mathrm{Cl}}, \mathcal{B}_{\mathrm{Cl}(3)}) = 0.191$ electron pairs (cf. Table 4.3). The sharing of electron between bonding basins is done mainly within the same valence basin

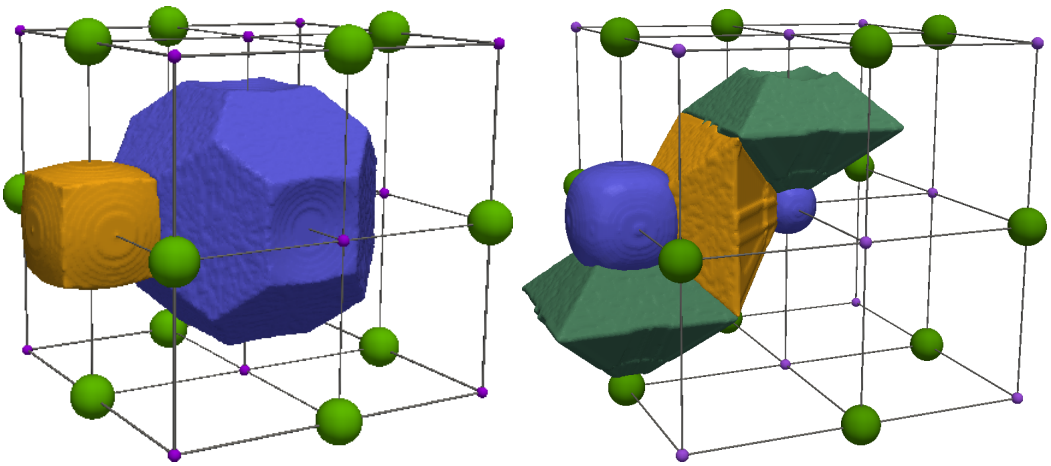

Figure 4.4.: LiCl QTAIM and ELI-D basins. Left: QTAIM atomic basin for Cl (blue) and Li (yellow). Right: ELI-D core basins for Cl $\mathcal{C}_{\mathrm{Cl}}$ (blue, small) and Li $\mathcal{C}_{\mathrm{Li}}$ (blue, large). Bonding ELI-D basins $\mathcal{B}_{\mathrm{Cl}(3)}$ are shown in yellow and green

set with DI $\delta(intra) = 0.276$ one order of magnitude larger than that for basins belonging to different valence basin sets $\delta(inter) = 0.012$. The fusion of the 6 bonding basins $\mathcal{B}_{\mathrm{Cl}(3)}$ around a Cl core is now justified.

As occurred in the NaF case the Cl core is surrounded by 6 bonding basins $\mathcal{B}_{\mathrm{Cl}(3)}$ (Fig. 4.4) that when merged together into a single superbasin closely resemble the QTAIM basin for the same atom (compare left, blue basin in Fig. 4.4 and right, light red basin in Fig. 4.3). The equivalence between both QTAIM and ELI-D basins should be supported by similar fraction of shared distant pairs ς (see Eq. 2.86).

Every superbasin shares electron pairs with the Cl atomic core it surrounds, with the 6 Li atomic cores is surrounded by as well as with the symmetry equivalent superbasins centered at each of the 12 Cl neighbouring atomic cores. In one line $\varsigma(\mathcal{S}[6\mathcal{B}_{\mathrm{Cl}(3)}]) = 2 \times 1.19 - (1.135 + 6 \times 0.032 + 12 \times 0.082) = 0.07$ (Table 4.2 and 4.4) which is very close to $\varsigma(\mathrm{Cl}) = 0.06$, hence supporting the close equivalence between the QTAIM Cl atomic basin and the ELI-D valence basin set.

The shape of the basins carries information abou to what extent this basin is chemically active. ELI-D basins provide a deeper insight into the chemical bonding situation of the crystal than the QTAIM basins do. The more simple picture offered by QTAIM where only atomic basins are shown treats equally the chemically inert electrons and the electrons participating in the bond. The analysis of a two-particle quantity performed by ELI-D allows to differentiate between distinct behaviours of the electrons.

The more spherical a basin is the lower its contribution to the formation of a

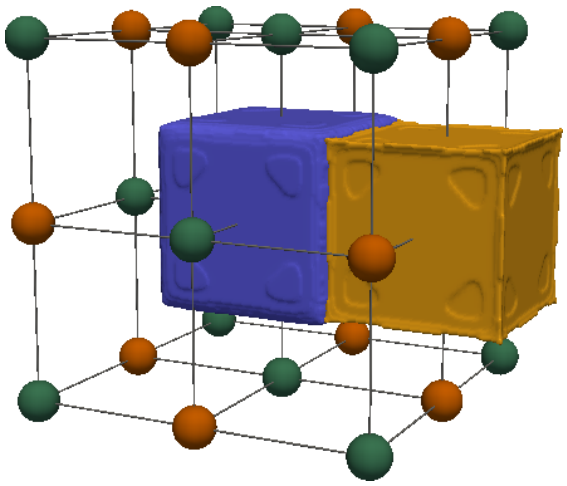

Figure 4.5.: SnTe QTAIM basins atomic basin for Sn (blue) and Te (yellow).

chemical bond. Consequently, atomic core basins are expected to have to a high extent an sphere-like shape; as can be seen in Fig. 4.1 (right), the blue core basin $\mathcal{C}_{\mathrm{K}}$ is almost a perfect sphere that includes the 1st and 2nd atomic shells of the K atom. The 3rd one is represented by the 24 bonding basins $\mathcal{B}_{4\mathrm{K}}$ of which only two (green and yellow) are shown (see Fig. 4.1, right).

In the cases of NaF and LiCl, the atoms mostly participating in bonding are F and Cl, respectively and their valence electrons are already forming part of the bonding ELI-D basins. The atomic core basin is only including the inner electrons that are not contributing to the bond and consequently the F and Cl atomic cores are prectially spheres (see the right part of Figs. 4.2 and 4.4, respectively). The atomic basins of the atoms acting as cations: Na and Li, are not so spherical as the aforementioned since although no bonding basin correspond to them, a certain contribution to the bond exists.

QTAIM atomic basins are even less spherical shaped than ELI-D ones for the Na and Li atoms. QTAIM analysis is less precise than ELI-D and each basin delimitates what is thought to be an atom, including both core and valence electrons. The higher contribution of the donor atoms (F and Cl) is seen by the very low sphericity of their corresponding basins (blue basins in the left part of Figs. 4.2 and 4.4, respectively). The basin for Na and Li (yellow ones in the same figures) resemble more a sphere and are alike the equivalent ELI-D core basins (blue, large in the right part).

4.3. Semiconductors: SnTe

QTAIM

Characteristic of metals is a high delocalization of the valence electrons since they are free to travel far away across the solid. In other words, the probability of finding an electron far from the nucleus it belongs to is very high. On the contrary, insulators are thought to have very localized electrons which are strongly linked to their nucleus and are not free to separate far from it, i.e., it is not expected to find a electron delocalized beyond the closest neighbourhood from its nucleus. Accordingly the distant shared pairs indicator $\varsigma(A)$ (Eq. 2.86) and the fraction of electrons shared with basins located beyond the nearest ones $\varkappa(A)$ (Eq. 2.87) are expected to be high for *bcc* K as a metal and low for NaF and LiCl as insulators. $\varsigma(K) = 0.88$ of the total shared pairs which means that a 55 % $\varkappa(K) = 0.55$ are shared with distant neighbours, that is over half of the shared electrons are dispersed across the solid (see Table 4.1). For the insulators the distant shared pairs values are one order of magnitude lower $\varsigma(Na) = 0.02$ and $\varsigma(Li) = 0.04$, with only a 4 % and 15 %, respectively, of the shared electrons delocalized far from their respective nucleus (Table 4.1).

As semiconductor SnTe is thought to occupy an intermediate position between *bcc* K and the ionic NaF and LiCl with a somewhat large distant delocalization but always below the metal value. As expected $\varsigma(K) = 0.88 > \varsigma(Sn) = 0.62 > \varsigma(Na) = 0.02 \approx \varsigma(Li) = 0.04$. A 19 % of the shared electrons can move away from their nucleus and be found delocalized among the solid.

The shape of the basins for SnTe follows again the rule mentioned above: the cations are rigid and as so occupy the space adquiring a convex shape (blue Sn basin in 4.5). On the contrary, the anions are distortable and behave fully occupying the free space left by the cations being concave (yellow Te basin in 4.5).

QTAIM LI and DI are shown in Table 4.1. The occupation number is now much higher than for the other systems considered here, which causes a higher fluctuation to occur $\sigma^2(Sn) = 1.62$ and $\sigma^2(Te) = 1.90$, which are around twice the fluctuation of the metal and four times that of the insulators. Each Sn atomic basin has a high DI value sharing $6 \times 0.40 = 2.4$ electrons with the nearest Te basins. But it is also important the DI between identical basins somewhat more distant $\delta(Sn - Sn) = 0.03$ and $\delta(Te - Te) = 0.07$.

Effect of the number of k-points in the ELI-D field

Due to the very demanding computational effort that entails the SnTe calculation with respect to the number of k-points, this parameter was reduced in small steps in order to get a fast enough though not very accurate performance. That allowed us to draw a representation of how the ELI-D field loses features as the

Brillouin Zone is progresively more coarse-grained sampled. In Fig. 4.6 can be seen that reducing the number of sampling points makes it impossible to solve the particularities that are contained between the k-points. There are features as the discs between second neighbour atoms in Fig. 4.6a that become smaller (Fig. 4.6b) until they fade away for k-points $= 2$ in Fig. 4.6c.

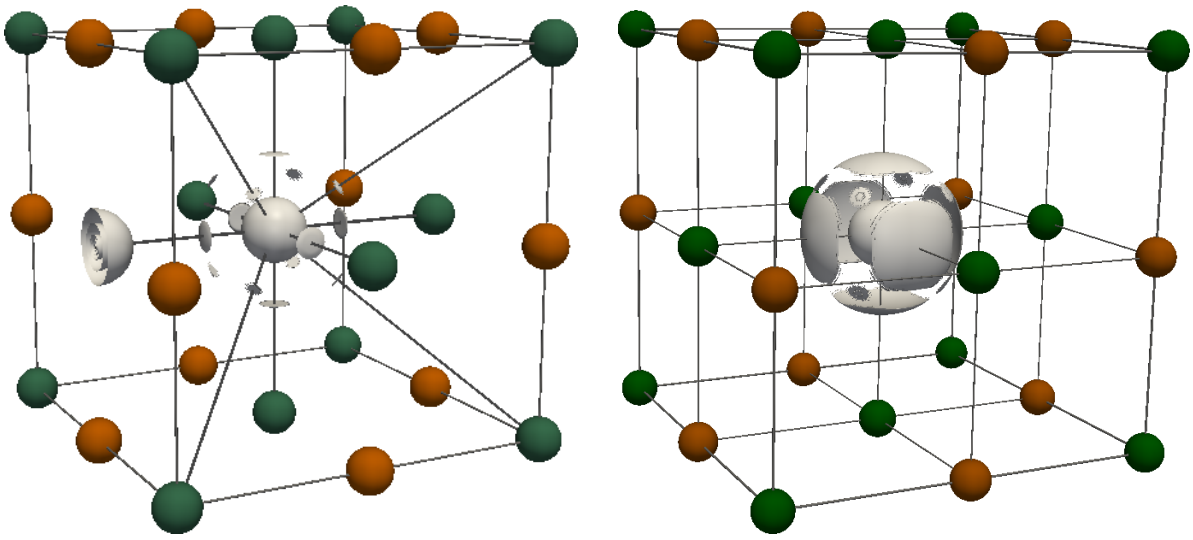

(a) k-points = 6

(b) k-points = 3

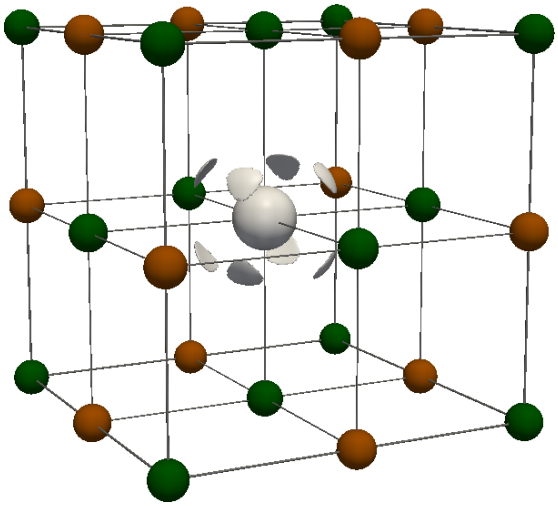

(c) k-points = 3

Figure 4.6.: ELI-D isosurfaces for $\Upsilon_D = 1.23$ using 6, 3 and 2 k-points, respectively. Note how the features lose complexity when lowering the accuracy of the calculation.

4.4. Topology of the electron density for bcc K, LiCl and SnTe

According to what was explained in section 2.3 the critical points (CP) of the electron density ρ defined within the QTAIM [3] have been analysed for *bcc* K, LiCl and SnTe. The CPs have been grouped according to the Wyckoff position they occupy and the points not determined by symmetry have been specified. Also the electron density ρ and the laplacian of the electron density $\nabla^2\rho$ are given. CPs of *bcc* K, whose symmetry is $Im\bar{3}m$ can be seen in Table 4.5 whilst those for LiCl and SnTe, symmetry $Fm\bar{3}m$ are in Table 4.6.

The translational invariant crystals are topologically equivalent to S^3, the 3-torus, and consequently all topological schemes must satisfy Morse invariant relationships [50], [51]:

$$n - b + r - c = 0, \tag{4.1}$$

and

$$n \geq 1, \quad b \geq 3, \quad r \geq 3, \quad c \geq 1, \tag{4.2}$$

where n is the total number of nuclei —or maxima or attractors— in the unit cell, b the number of bonds, r the number of rings and c the number of cages or minima. We consider also the number of symmetrically different nuclei in the unit cell τ_n and similarly τ_b, τ_r and τ_c for bond, ring and cage CPs. This information is given in the vector form $\boldsymbol{\tau} = (\tau_n, \tau_b, \tau_r, \tau_c)$:

$$\tau = \tau_n + \tau_b + \tau_r + \tau_c.$$

The traditional classification of the different types of chemical bond in solids into Covalent, Ionic and Metallic can be quantitatively done by means of an topological analysis of the electron density [52]. Ionic crystals are divided into basins containing a substantial net charge close to the nominal oxidation state and exhibiting small electron density ρ_b and positive laplacian $\nabla^2\rho_b$ at the bond CPs (BCP). Positive laplacian corresponds to regions of charge depletion which occurs in the ionic picture where linkage is due to closed-shell charge-depletion interactions. Negative laplacian indicates regions of local charge accumulation. Accordingly covalent solids have large electron density values at the BCP and negative density laplacian. The trird type of chemical bond, the metallic solids show valence electrons scattered throughout the solid yielding very low values of both ρ_b and $\nabla^2\rho_b$.

Table 4.5.: Topological scheme of the CP's of the electronic density for K *bcc*. The space group is $Im\bar{3}m$. The type of CP is listed as n: nuclei, c: cage, b: bond and r: ring. Electron density $\rho[=]electron\ bohr^{-3}$ and $\nabla^2\rho$ values at each point are written in the last two columns.

Wyckoff	Symmetry	Position	K *bcc*	ρ	$\nabla^2\rho$
2a	m$\bar{3}$m	$(0,0,0)$	n: K	6059.902	-
6b	4/mm.m	$(0,1/2,1/2)$	c	0.0025	0.0002
8c	.$\bar{3}$m	$(1/4,1/4,1/4)$	b	0.0025	0.0006
12d	$\bar{4}$m.2	$(1/4,0,1/2)$	r	0.0023	0.0001
$(\tau_n,\tau_b,\tau_r,\tau_c)$ index			(1,1,1,1)		
Number of critical points (τ)			4		

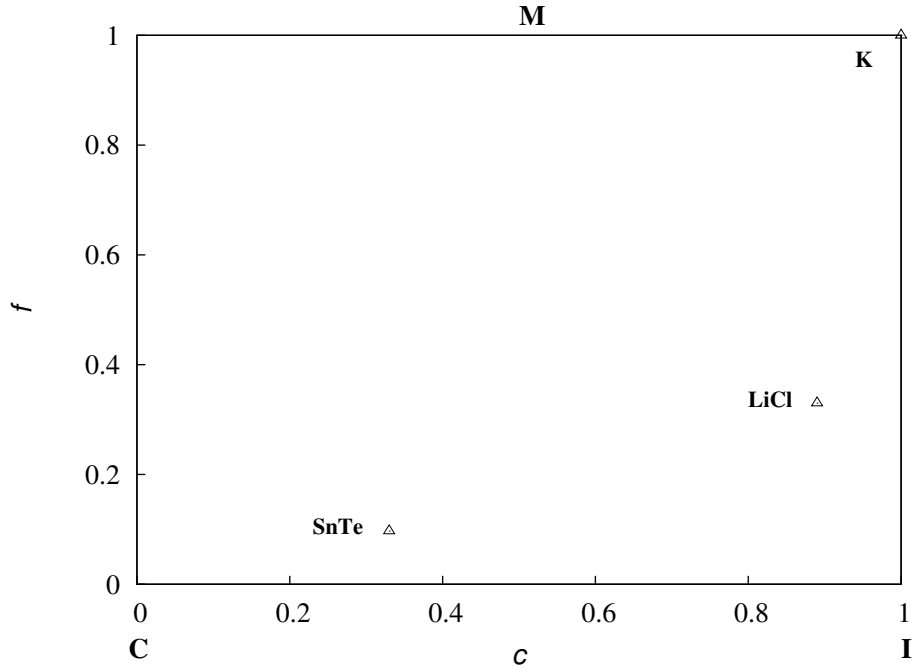

Figure 4.7.: Flatness Vs. charge-transfer diagram for *bcc* K, LiCl and SnTe as metallic, ionic and covalent crystals, respectively.

Table 4.6.: Topological scheme of the CP's of the electronic density of LiCl and SnTe. The space group is $Fm\bar{3}m$. Float numbers in parenthesis represent the x, y and z coordinates not fixed by symmetry. The type of CP is designated according to n: nuclei $(3,-3)$, c: cage $(3,+3)$, b: bond $(3,-1)$ and r: ring $(3,+1)$. Electron density $\rho[=]electron\,bohr^{-3}$ and $\nabla^2\rho$ values at each point are written in the last column.

Wyckoff	Symmetry	Position	LiCl	ρ	$\nabla^2\rho$	SnTe	ρ	$\nabla^2\rho$
4a	m$\bar{3}$m	(0,0,0)	n: Li	13.548	-	n: Sn	5.416E5	-
4b	m$\bar{3}$m	(1/2,1/2,1/2)	n: Cl	4.702E3	-	n: Te	7.079E5	-
8c	$\bar{4}$3m	(1/4,1/4,1/4)	c	0.004	0.011	c	0.003	0.006
24d	m.mm	(0,1/4,1/4)	b	0.009	0.022	r	0.008	0.014
24e	4m.m	(x,0,0)	b: (1.660)	0.012	0.049	b: (2.816)	0.031	0.025
48h	m.m2	(0,y,y)	r: (1.393)	0.007	0.023			
$(\tau_n,\tau_b,\tau_r,\tau_c)$ index			(2,2,1,1)			(2,1,1,1)		
Number of critical points (τ)			6			5		

Ionic compounds such as LiCl present low electron density $\rho_b(\text{LiCl}) = 0.012$ at the BCP and positive density laplacian $\nabla^2\rho_b(\text{LiCl}) = 0.049$ (Table 4.6. In the polar case of SnTe the density is larger $\rho_b(\text{SnTe}) = 0.031$ as but although the density laplacian is also positive (Table 4.6). On the contrary the metallic solid *bcc* K has very low density values $\rho_b(\text{K}) = 0.0025$ and very low values of the density laplacian $\nabla^2\rho_b(\text{K}) = 0.006$ (Table 4.5). The metallic character of *bcc* K is also confirmed by the value of the density that has a constant value no matter the CP where it has been evaluated.

An over 50 year-old chemical bond classification method was proposed by van Arkel and Ketelaar [53], [54]. It is known as the van Arkel-Ketelaar diagram (VK) and has been shown to be recovered from the electron density without explicitly reference to any empirical scales [52]. It is a covalent-ionic-metallic triangular diagram that allows a classification of the chemical bond into the traditional types. The covalence-ionicity of the AB compound is given by the difference in electronegativity $|\chi_A - \chi_B|$. On the other hand, the metallicity-covalency character is given by the average $(\chi_A + \chi_B)/2$.

The ρ-based way of constructing this triangle is defined in [52] from the flatness f and charge transfer c indices. Characteristic of metallic systems is a flat electron density defined as

$$f = \frac{\rho_c^{min}}{\rho_b^{max}}, \tag{4.3}$$

where ρ_c^{min} is the absolute minimum of the electron density at a cage CP and ρ_b^{max} is the absolute maximum of the electron density at a bond CP. This index allows the separation between metals ($f \approx 1$) and nonmetals ($f \approx 0$) by exploiting the idea that the relevant part of the valence electron density starts at the highest BCP and finishes at the lowest density cage critical point.

The other coordinate is defined according to a charge transfer scale calculated as

$$c = \frac{1}{N}\sum_{\Omega}^{N}\frac{\mathcal{L}(\Omega)}{\text{OS}(\Omega)} = \left\langle \frac{\mathcal{L}(\Omega)}{\text{OS}(\Omega)} \right\rangle. \tag{4.4}$$

That expression is an averaged of the ratios between the topological charge $\mathcal{L}(\Omega)$ and the nominal oxidation state $\text{OS}(\Omega)$ for every basin Ω which measures how much this basin deviates from the ideal ionic model.

The VK triangle defined plotting the charge-transfer against the flatness is shown for our systems in Fig. 4.7. The labels of the corners indicate where ideal covalent (C) and ionic (I) crystals are situated, while (M) indicates that the upper part of the figure is occupied by metals. The semiconductor SnTe is close to the covalent corner while LiCl approximates the ionic one. The mentioned nature of

the chemical bond in crystals is hence confirmed and the usefulness of the VK-like triangle to determine it.

5. Conclusiones

El objetivo de este trabajo ha sido tomar contacto con algunas técnicas novedosas para estudiar el enlace químico en el espacio real.

Las conclusiones más relevantes son:

1. La conclusión fundamental que podemos extraer de este trabajo tiene relación con el Indicador de Localizabilidad Electrónica ELI-D. Esta función supone una alternativa a la ya clásica ELF y como ésta permite la resolución de la estructura de capas atómicas de las especies que se encuentran formando un sistema químico. A partir de esta función, construida a partir de la densidad de parejas electrónicas, se puede hacer una una partición más fina del espacio de la hecha de acuerdo a la QTAIM, basada en la densidad electrónica. Mientras que la división del espacio según QTAIM resulta en cuencas que se hacen corresponder con átomos —exceptuando el caso de máximos no nucleares—, la función ELI-D permite partir el volumen ocupado por el sistema en regiones llamadas "dominios de localización" (*localization domains*), que se interpretan como correspondientes con regiones de enlace, núcleos atómicos y pares solitarios. De esta manera, mientras que QTAIM nos permite visualizar la únidad atómica, concepto que sirve de sustento a la química, creando cuencas que ocupan todo el espacio y se hacen corresponder con los núcleos atómicos, ELI-D nos permite ir más allá y partir el dominio atómico en una parte químicamente inerte —núcleos atómicos—, una activa que interviene en el enlace —región de valencia— y en caso de existir un volumen de pares solitarios. Es importante destacar que a esta partición no se le ha encontrado aún significado físico alguno, está en cambio motivada por analogía con la realizada de acuerdo con la QTAIM.

2. Los índices de localización y deslocalización son herramientas ya establecidas que permiten una caracterización cuantitativa del enlace químico. Su evaluación dentro de las cuencas en que, de acuerdo con ELI-D, fue dividido el espacio proporciona información sobre el tipo de enlace existente entre los átomos. Así, de acuerdo con la medida que los índices proporcionan de cómo de localizados están los electrones en cada cuenca, podremos clasificar la región de enlace como correspondiente a un enlace covalente, un enlace iónico o uno metálico. Los sistemas escogidos: *bcc* K, NaF, LiCl y SnTe intentan ofrecer un ejemplo de cada uno de los mencionados tipos de enlace

y sirven a su vez como otra demostración más de lo oportuno de aplicar ya bien QTAIM como ELI-D a sistemas en fase condensada.

3. La disponibilidad de índices de localización o deslocalización en sólidos abre vías interesantes de análisis que hasta ahora han permanecido cerrados. Como hemos mostrado en sistemas modelo, los valores obtenidos son consistentes con la intuición. Pretendemos proseguir con este estudio en el futuro.

6. Bibliography

[1] M. Kohout, "DGrid 4.6," (Radebeul, 2012).

[2] P. Hohenberg and W. Kohn, Physical Review **136**, B864 (1964).

[3] R. Bader, *Atoms in Molecules: A Quantum Theory*, International Series of Monographs on Chemistry (Clarendon Press, 1994).

[4] R. Daudel, H. Brion, and S. Odiot, The Journal of Chemical Physics **23**, 2080 (1955).

[5] R. Daudel, *The fundamentals of theoretical chemistry: wave mechanics applied to the study of atoms and molecules* (Pergamon, 1968).

[6] R. Bader and M. Stephens, Journal of the American Chemical Society **97**, 7391 (1975).

[7] J. Lennard-Jones, Proceedings of the Royal Society of London. Series A. Mathematical and Physical Sciences **198**, 14 (1949).

[8] M. Kohout, International journal of quantum chemistry **97**, 651 (2004).

[9] M. Kohout, F. Wagner, and Y. Grin, International journal of quantum chemistry **106**, 1499 (2006).

[10] M. Kohout, Faraday Discuss. **135**, 43 (2006).

[11] A. Pendás, A. Costales, and V. Luaña, Physical Review B **55**, 4275 (1997).

[12] V. Luaña, A. Costales, and A. Pendás, Physical Review B **55**, 4285 (1997).

[13] A. Pendás, A. Costales, and V. Luaña, The Journal of Physical Chemistry B **102**, 6937 (1998).

[14] A. Baranov and M. Kohout, Journal of Physics and Chemistry of Solids **71**, 1350 (2010).

[15] A. Baranov and M. Kohout, Journal of Computational Chemistry **29**, 2161 (2008).

[16] "Elk 1.4.18," (2012).

[17] A. Szabo and N. Ostlund, *Modern quantum chemistry: introduction to advanced electronic structure theory* (Dover Pubns, 1996).

[18] W. Koch and M. Holthausen, *A chemist's guide to density functional theory*, Vol. 2 (Wiley Online Library, 2001).

[19] L. Piela, *Ideas of quantum chemistry* (Elsevier Science, 2006).

[20] D. Griffiths and E. Harris, *Introduction to quantum mechanics*, Vol. 2 (Prentice Hall, 1995).

[21] C. Cohen-Tannoudji, B. Diu, and F. Laloë, *Quantum mechanics. (Mécanique quantique). Vol. 1-2.*, Quantum Mechanics (Wiley, 1977).

[22] W. Kohn and L. Sham, Phys. Rev **140**, A1133 (1965).

[23] S. Cottenier, *Density Functional Theory and the family of (L) APW-methods: a step-by-step introduction* (to be found at http://www.wien2k.at/reg_user/textbooks, (Instituut Voor Kern-en Stralingsfysica, KU Leuven, Belgium), 2004).

[24] K. Burke, *the ABC of DFT* (Rutgers University, 2007).

[25] H. Eschrig, *The Fundamentals of Density Functional Theory (revised and extended version)*, Vol. 9 (Edition am Gutenbergplatz, Leipzig, Germany, 2003).

[26] R. McWeeny and B. Sutcliffe, *Methods of molecular quantum mechanics*, Vol. 2 (Academic Press London, 1969).

[27] R. Bader, Chemical Reviews **91**, 893 (1991).

[28] A. Pendás, M. Blanco, A. Costales, P. Sánchez, and V. Luaña, Physical review letters **83**, 1930 (1999).

[29] A. Pendás, M. Kohout, M. Blanco, and E. Francisco, in *Modern Charge-Density Analysis*, edited by C. Gatti and P. Macchi (Springer Verlag, 2012) pp. 303–782.

[30] J. Dobson, Journal of Chemical Physics **94**, 4328 (1991).

[31] R. Gillespie, *Molecular geometry* (Van Nostrand Reinhold London, 1972).

[32] B. Silvi and A. Savin, Nature **371**, 683 (1994).

[33] A. Becke and K. Edgecombe, Journal of Chemical Physics **92**, 5397 (1990).

[34] R. Bader and M. Stephens, Chemical Physics Letters **26**, 445 (1974).

[35] R. Bader, A. Streitwieser, A. Neuhaus, K. Laidig, and P. Speers, Journal of the American Chemical Society **118**, 4959 (1996).

[36] X. Fradera, J. Poater, M. Duran, and M. Solà, Chemistry-a European Journal **9**, 400 (2003).

[37] X. Fradera, J. Poater, S. Simon, M. Duran, and M. Sola, Theoretical Chemistry Accounts: Theory, Computation, and Modeling (Theoretica Chimica Acta) **108**, 214 (2002).

[38] X. Fradera, M. Austen, and R. Bader, The Journal of Physical Chemistry A **103**, 304 (1999).

[39] A. Baranov and M. Kohout, J. of Comput. Chem. **32**, 2064 (2011).

[40] J. Angyan, M. Loos, and I. Mayer, The Journal of Physical Chemistry **98**, 5244 (1994).

[41] R. Ponec, Theoretical Chemistry Accounts: Theory, Computation, and Modeling (Theoretica Chimica Acta) **114**, 208 (2005).

[42] C. Ambrosch-Draxl, Physica Scripta **T109**, 48 (2004).

[43] J. Slater, Physical Review **51**, 846 (1937).

[44] O. Andersen, Physical Review B **12**, 3060 (1975).

[45] D. Koelling and G. Arbman, Journal of Physics F: Metal Physics **5**, 2041 (1975).

[46] D. Singh, Physical Review B **43**, 6388 (1991).

[47] E. Sjöstedt, L. Nordström, and D. Singh, Solid State Communications **114**, 15 (2000).

[48] "Paraview: a parallel visualization application," Sandia National Labs and Kitware Inc. and Los Alamos National Labs. (2000-2008), version 1.14.1.

[49] A. McNaught, A. Wilkinson, I. U. of Pure, and A. Chemistry, *IUPAC Compendium of Chemical Terminology* (Blackwell Scientific Publications, Oxford, 1997).

[50] M. Morse and S. Cairns, *Critical point theory in global analysis and differential topology: An introduction*, Vol. 33 (Academic Press, 1969).

[51] W. Jones and N. March, *Theoretical solid state physics: Perfect lattices in equilibrium*, Vol. 1 (Dover Pubns, 1985).

[52] P. Mori-Sánchez, A. Pendás, and V. Luaña, Journal of the American Chemical Society **124**, 14721 (2002).

[53] A. Arkel, Interscience, New York (1956).

[54] J. Ketelaar, *Chemical constitution: an introduction to the theory of the chemical bond* (Elsevier, 1953).

A. DGrid input files

We will shortly describe here how to use the software DGrid 4.6 to obtain a field of a chosen property —as the electron density— from a single point solid state calculation with the Elk code. Using the property file further analysis can be done:

- space partitioning according to the chosen property
- evaluation of overlap integrals which Localization (LI) and Delocalization Indices (DI) can be obtained from
- topological analysis of the property, i.e., search for critical points

Starting from the solid state calculation results, the process can be regarded as be formed by a few steps that must be consecutevely executed. Each of the following Sections stands for a calculation that is dependent of the preceeding ones and will be needed for further evaluations. They must hence be executed in the order given here. Within a Section some subsections can be found that are at the same level and consequently can be independently calculated. LiCl $Fm\bar{3}m$ will be used as an example. Note that only explanations in relation to the transcribed inputs are given. For a further detailed description the reader is referred to the user's guide, which can be downloaded from [1].

A.1. PREVIOUS STEP: Elk output transformation

DGrid 4.6 [1] is a software that computes properties for solid state systems on a 3-dimensional grid from the data from the full potentail solid state code Elk [16]. Before we start any DGrid solid state calculation we must generate the file containing the information needed from the Elk calculation for a property evaluation. DGrid has to be run in the same folder where the Elk output files are located and the Elk input file will be given as DGrid input:

```
dgrid elk.in licl.mte
```

A resulting `.mte` file is constructed.

A.2. STEP 1: Property file

The first step will consist in the construction a 3-dimensional grid with a value of the chosen property at every grid point. Not only one but many properties can be evaluated at the same time. The DGrid input file is as follows:

```
:TITLE
:-----------------------------------------------|
::LiCl  elk default
:-----------------------------------------------|

:KEYWORDS
:-----------------------------------------------
basis=licl.mte

output=.

:CHOOSE THE DESIRED PROPERTIES
:-----------------------------------------------
compute=rho
compute=ELI-D alpha-alpha
:-----------------------------------------------

 GRID_DEFINITION:       vectors
:             X      Y      Z
:------------------------------
 origin:    0.0    0.0    0.0
:                                    INTERVALS
:---------------------------------------------
 i-vector:  4.8467 0.0    0.0          97
 j-vector:  0.0    4.8467 0.0          97
 k-vector:  0.0    0.0    4.8467       97

END
```

The input consists of various parts:

TITLE consists of a comment of the calculation that will be done. With `elk default` we make clear that we have used the basis set given in Elk by default.

KEYWORDS is the part where we give DGrid instructions of how do work. `basis` will always be a `name.mte` file for solid state calculations. `output` defines where do we want to save the output. A dot indicates it will use the embedded pattern to create the name of the file (see below).

PROPERTIES is where we give DGrid the properties we want. In our case only the electron density and the ELI-D for same up-spin. Consult the manual for more details.

GRID_DEFINITION since we are facing a solid state calculation, the volume where we want to perform the calculation has to be specified. First we define a origin which is the reference point from where the i, j and k vectors are defined. On the interest of time, only 1/8 of the LiCl unit cell is evaluated ($cell$ = 9.6934 a. u.), which afterwards will be mirrored to get the whole cell. In the `INTERVALS` column we define how fine do we want the grid to be. Here each grid point will be at 0.05 bohr from the following one.

input file: "1_licl_dg.inp"
output file: "licl.mte.dg" containing information about the calculation: timing, atom positions...
property file: "licl.mte.rho_r" and "licl.mte.elid_r_a_aa" containing the result —electron density and ELI-D grid, respectively—.

Whole unit cell formation In order to recover the whole unit cell from the 1/8th calculated, DGrid has a utility that mirrors the data along each of the axis. Since the mirroring operation is a really fast process a lot of computational time is saved. The operation is invoked by:

```
dgrid licl.mte.rho_r op1
```

Once the interactive dialog is opened the `mirror in` will do the mirroring along the i direction. The `n` just specifies that the mirroring is done from the end of the small cell, unlike `mirror i` that makes the operation to be done from the begining.

A.3. STEP 2: Space partitioning

From the files containing a grid with the electron density and ELI-D for LiCl a partition of the space in basins can be performed. DGrid input is as follows:

```
:TITLE
:-------------------------------------------------------------|
:: LiCl ELI-D alpha-alpha basins
:-------------------------------------------------------------|

:KEYWORDS
:-------------------------------------------------------------
property =licl.mte.elid_r_a_aa
```

```
integrate=licl.mte.rho_r

output=.

top=1.5
eli_core
symmetry=translation i j k

END
```

This input file tells DGrid to search for basins according to the `property` keyword and integrates `integrate` within them. For the input to calculate the QTAIM basins the same density `.rho_r` file is given in both keywords.

top is a variable which permits the control of how many basins are created. A good description of how this keyword works is given in the user's guide which can be downloaded from the program web site free of charge [1]. To decide at which value basins corresponding to irreducible domains are drawn it is recomended to have a look at isosurfaces of the property. With the visualization software ParaView [48] it can be seen for what ELI-D value the localization domains can not further bifurcate.

eli_core is a keyword that avoids the formation of numerous basins close to the nucleus. Up to a internally defined radius all basins are assigned to the atomic core basin.

symmetry is another variable indicating that the system is symmetrical in the three dimensions. It tells DGrid to automatically assign symmetrically equivalent basins to the same one.

input file: "2_bas_licl_elidaa.inp"
output file: "licl.mte.elid_r_a_aa.bas"
property file: "licl.mte.elid_r_a_aa.bsn"

The respective files are created for the remaining calculated properties.

A.4. STEP 3

A.4.1. Overlap integrals evaluation

Once the basins have been created, the overlap integrals within each of them can be evaluated and the LI and DI calculated.

```
:TITLE
:-------------------------------------------------------------|
:: LiCl overlap over ELI-D basins
:-------------------------------------------------------------|

:KEYWORDS
:-------------------------------------------------------------
property=licl.mte.elid_r_a_aa.bsn
integrate=licl.mte.rho_r

output=.

overlap
symmetry=translation  i  j  k
:basin_mte = 8    80.0

END
```

Similarly as in the previous step, the `integrate` keyword tells DGrid what whould be integrated within each basin of the while the determined by the keyword `property`: ELI-D basins in this example. The corresponding `.rho_r.bsn` file would be introduced for LI and DI over Bader basins.

overlap is the keyword indicating the code it must calculate overlap integrals using the above files.

basin_mte default values are 30 and 50.0. First value controls the expansion size of the multipole whilst the second regulates the Fourier expansions of the basin shape. Note it is commented out here by the colon.

input file: "3_ovl_licl_elidaa.inp"
output file: "licl.mte.elid_r_a_aa.ovl" where the "pair density analysis" section includes LI and DI.
property file: "licl.mte.elid_r_a_aa.sij" containing the overlap integrals.

A.4.2. Critical points search

Once the basins were found a topological analysis of the property can be performed. It consists of a search for critical points of the field according to the rank and signature of the hessian for the considered property. According to that attractors, repellors and saddle points can be found.

```
:TITLE
:-------------------------------------------------------------|
```

```
:: LiCl ELI-D topology
:-------------------------------------------------------------|

:KEYWORDS
:-------------------------------------------------------------
property =licl.mte.elid_r_a_aa.bsn

output=.

eli_core
topology
:icl_graph=full

END
```

topology is the keyword that we need to specify the program in order to perform a topological analysis of the ELI-D basins.

icl_graph tells the program to find the interconnection paths between all the critical points searched. However only a particular type of CP can be interconnected, as for example the saddle points or the bond points. The resulting paths can be visualized with ParaView.